Title

Inter-organelle crosstalk supports acetyl-coenzyme A homeostasis and lipogenesis under metabolic stress

Short title**:** Peroxisomal metabolism supports acetyl-CoA homeostasis and lipid synthesis

Authors

Ramya S Kuna[1,2#], Avi Kumar[1,2#], Karl A Wessendorf-Rodriguez[1,2], Hector Galvez[1], Courtney R Green[1,2], Grace H McGregor[1,2], Thekla Cordes[1,2,4], Reuben J Shaw[1], Robert U Svensson[3], Christian M Metallo[1,2]*

Affiliations

[1] Department of Molecular and Cell Biology, Salk Institute for Biological Studies, La Jolla, CA 92037, USA

[2] Department of Bioengineering, University of California, San Diego, La Jolla, CA 92093, USA

[3]Nimbus Therapeutics, Cambridge, MA 02139, USA

[4]Department of Bioinformatics and Biochemistry, Braunschweig Integrated Centre of Systems Biology (BRICS), Technische Universität Braunschweig, Braunschweig 38106, Germany

# Ramya S Kuna and Avi Kumar contributed equally to this article.

*Corresponding author

Correspondence: metallo@salk.edu

Abstract

Proliferating cells rely on acetyl-CoA to support membrane biogenesis and acetylation. Several organelle-specific pathways are available for provision of acetyl-CoA as nutrient availability fluctuates, so understanding how cells maintain acetyl-CoA homeostasis under such stresses is critically important. To this end we applied ^{13}C isotope tracing cell lines deficient in these mitochondrial (ATP-citrate lyase; ACLY-), cytosolic, (acetyl-CoA synthetase (ACSS2-), and peroxisomal (peroxisomal biogenesis factor 5; PEX5-) dependent pathways. ACLY knockout in multiple cell lines reduced fatty acid synthesis and increased reliance on extracellular lipids or acetate. Knockout of both ACLY and ACSS2 (DKO) severely stunted but did not entirely block proliferation, suggesting alternate pathways can support acetyl-CoA homeostasis. Metabolic tracing and PEX5 knockout studies link peroxisomal oxidation of exogenous lipids as a major source of acetyl-CoA for lipogenesis and histone acetylation in cells lacking ACLY, highlighting a role for inter-organelle crosstalk in supporting cell survival in response to nutrient fluctuations.

Teaser

ATP-citrate lyase deficiency highlights critical sources of lipogenic acetyl-CoA in cancer cells

MAIN TEXT

Introduction

Acetyl-CoA is a critical precursor for acetylation and lipid synthesis associated with membrane biogenesis, energy storage, and protein modification (*1*). Central carbon metabolism is wired with several redundancies in place to maintain acetyl-CoA homeostasis under conditions of stress, with mitochondria, peroxisomes, and cytosolic acetate activation all contributing to this metabolic pool. While both healthy tissues and tumors readily incorporate lipids from the diet (*1*), *de novo* lipogenesis (*DNL*) is required for some tumors and cell types to proliferate (*2*, *3*), how each of these pathways and organelles fuel lipogenesis is not fully clear. Fatty acids are synthesized from two carbon acyl-units provided by cytosolic acetyl-CoA, which is metabolized to malonyl-CoA by acetyl-CoA Carboxylase (ACC) and used by fatty acid synthase (FASN) to generate long-chain fatty acids. These fatty acids can be further elongated, desaturated, and incorporated into lipids within the endoplasmic reticulum (ER). In the context of cancer, FASN inhibition reduces body weight (*4*), oncogene expression (*5*), and *in vivo* growth (*6*) of human breast cancer cell lines in mice. Knockout and pharmacological inhibition of acetyl-CoA carboxylase also compromise tumor growth in xenograft and genetically-engineered mouse models of lung cancer while synergizing with chemotherapy (*7*).

ATP-citrate lyase (ACLY) is the major conduit through which mitochondrial metabolism supports acetyl-CoA generation, which is important for lipid synthesis as well as epigenetic regulation and DNA repair via histone acetylation (*8–10*). Upregulation of ACLY expression has been identified in a number of numerous cancers upregulate ACLY expression compared to surrounding healthy tissue, including breast, liver, bladder, stomach, colorectal, glioblastoma, and lung cancers (*11–17*), and in patients with gastric adenocarcinoma (*18*) and lung adenocarcinomas (*17*), overexpression and activation of ACLY is associated with poor prognosis. Further, both pharmacological inhibition and genetic knockdown of ACLY have been demonstrated to reduce lipogenesis and cancer cell proliferation (*19–26*), supporting the link between ACLY activity and tumor growth. On the other hand, nutrient availability and mitochondrial metabolism are sometimes compromised in cells within the tumor microenvironment, and pathways like reductive carboxylation are often unable to fully compensate (*27*, *28*). Therefore, characterization of alternative acetyl-CoA sources may useful for understanding cancer cell survival and resistance mechanisms.

The acetyl-CoA synthetase family of enzymes (ACSS1, ACSS2, and ACSS3) are the rate limiting enzymes involved in acetate activation to acetyl-CoA in mammalian cells (*29*). While ACSS1 and ACSS3 are mitochondrially expressed and tissue-restricted (in the case of ACSS3), ACSS2 is localized in the cytosol (*30*). ACSS2 has garnered interest as a cancer target as high expression of ACSS2 is associated with poor prognosis in breast, glioblastoma, ovarian, and lung cancers (*31–33*). Nutrient deprivation, including hypoxia and lipid depletion, upregulate ACSS2 expression and acetate catabolism for DNL in cancer cells, suggesting that ACSS2 provides a mode of metabolic plasticity to cancer cells under stress (*34*). Hepatocyte selective depletion of ACSS2 or ACLY decreased liver acetyl-CoA levels in obese mice (*35*). Furthermore, mouse embryonic fibroblasts (MEFs) deficient in ACLY upregulate ACSS2 protein expression and increase utilization of acetate for cytosolic acetyl-CoA generation (*36*), highlighting the essentiality of acetyl-CoA and metabolic flexibility of proliferative cells.

Peroxisomes generate acetyl-CoA via β-oxidation of fatty acids, most often very long-chain (VLCFA) or branched-chain fatty acids (BCFA), which contribute to malonyl-CoA and lipids in the heart and liver (*37–40*). Peroxisomal enzymes involved in oxidation of BCFA (hydroxysteroid

17-beta dehydrogenase 4 (HSD17B4), Acyl-Coenzyme A Oxidase 3 (ACOX3)) are overexpressed in cancerous prostate tissue compared to paired healthy tissue (*41*), suggesting this organelle may support generation of acetyl-CoA in tumors. However, the extent to which peroxisomal β-oxidation of fatty acids serves as a source of lipogenic acetyl-CoA in cancer cells under nutrient stress warrants further exploration.

Here we apply mass spectrometry, stable isotope tracing and isotopomer spectral analysis (ISA) to analyze the metabolic rewiring that occurs when acetyl-CoA synthesis is systematically compromised in cancer cells. We genetically engineered cancer cell lines deficient in ACLY and/or ACSS2 using CRISPR/Cas9. While knockout of ACLY decreased *DNL* under basal conditions, cells are able to sustain FASN flux and/or growth through use of exogenous acetate or serum lipids. On the other hand, knockout of both ACLY and ACSS2 induces a growth limiting stress regardless of medium nutrient status. Finally, we observe that ACLY-deficient cells use peroxisomal β-oxidation as a significant source of lipogenic acetyl-CoA and are sensitive to peroxisomal biogenesis factor 5 (PEX5) knockout or pharmacological inhibition of peroxisomal β-oxidation. Collectively, our study highlights the rewiring of organelle-specific acetyl-CoA metabolism in fueling DNL when mitochondrial (ACLY), cytosolic (ACSS2), and peroxisomal (PEX5) CoA sources are compromised in cancer cells.

Results

ACLY deficiency compromises fatty acid synthesis and drives lipid-dependence of cell lines

ACLY-knockout (*ACLY*-KO) clones were generated using CRISPR/Cas9 in A549 human non-small-cell lung cancer (NSCLC) cells, 634T murine NSCLC cells, HepG2 hepatocarcinoma cells, and HAP1 cells (Fig. 1B, S1A). We observed increased protein expression of ACSS2 in the A549 and HepG2 *ACLY*-KO cell lines (Fig. 1B, S1A), consistent with previous results in MEFs (*36*). The growth rate of the *ACLY*-KO A549, 634T, and HAP1 cells was marginally lower compared to wildtype cells, while HepG2 *ACLY*-KO cells showed an over 50% reduction in growth rate compared to the wildtype cells (Fig. 1C, S1B). In A549 cells, *ACLY*-KO resulted in decreased glucose uptake/lactate secretion and increased glutamine uptake/glutamate secretion, suggesting rewiring of central carbon metabolism (Fig. 1D). To better understand how ACLY-deficiency alters intracellular metabolism, we cultured A549 clones in the presence of [U-$^{13}C_6$]glucose or [U-$^{13}C_5$]glutamine and quantified isotope enrichment in downstream metabolite pools. Enrichment of tricarboxylic acid (TCA) cycle intermediates from glutamine in A549 *ACLY*-KO cells was elevated, consistent with extracellular flux results (Fig.1E). These findings may indicate that ACLY-KO induces oxidative stress, as increased glutamine catabolism has been found to be integral to maintaining redox homeostasis in cancer cells through multiple mechanisms (*42*, *43*). On the other hand, glucose enrichment in malate and aspartate (a readout of oxaloacetate) was increased, likely due to decreased generation of acetyl-CoA via ACLY and glutamine-dependent reductive carboxylation (Fig. S1C). Schematic metabolic concept depicting the pyruvate-citrate shuttle and fatty acid synthesis (Fig. 1A).

HepG2 cells express the plasma membrane citrate transporter solute carrier family 13 member 5 (SLC13A5) (*44*), so we next used [2,4-$^{13}C_2$]citrate to directly trace the ACLY reaction in HepG2 *ACLY*-KO cells. Catabolism of [2,4-$^{13}C_2$]citrate provides insight into compartment-specific metabolism as M2 labeling of TCA intermediates will result from direct mitochondrial catabolism of labeled citrate, while M1 isotopologues will be formed if the tracer is first catabolized in the cytosol by ACLY (Fig. S1D). When culturing HepG2 wildtype and *ACLY*-KO cells in the presence of 500 μM [2,4-$^{13}C_2$]citrate, we found the ratio of M1/M2 labeling on malate, aspartate, succinate, and fumarate was significantly decreased in the *ACLY*-KO cells (Fig. S1E). Furthermore, the

relative abundance of M2 alpha-ketoglutarate was comparable to M1 labeling in wildtype cells but was significantly greater in the *ACLY*-KO cells (Fig. S1F). Additionally, enrichment of palmitate was minimal in the *ACLY*-KO cells compared to wildtype (Fig. S1G). These labeling patterns confirm that *ACLY*-KO forces cells to oxidize citrate in the mitochondria and/or cytosol to alpha-ketoglutarate at the expense of acetyl-CoA generation. Next, we applied ISA to quantify palmitate synthesis and the contribution of [U-$^{13}C_6$]glucose to the lipogenic acetyl-CoA pool. ACLY-deficiency profoundly decreased palmitate synthesis compared to control cells (Fig. 1F, S1H, I). Notably, *ACLY*-KO cells maintained some flux from [U-$^{13}C_6$]glucose to lipogenic acetyl-CoA such that ~20% of palmitate carbon was derived from glucose in A549 and HepG2 cells, while a smaller decrease was observed in 634T cells (Fig 1G, S1J). Collectively, these results indicate that ACLY deficiency effectively decreases FASN flux and alters cytosolic citrate shuttling under normal culture conditions while reducing growth slightly.

Acetate metabolism by ACSS2 supports lipogenesis to enable growth of ACLY-deficient cells

Under conditions where glucose-derived citrate is limiting, such as hypoxia, acetate can be "activated" by acetyl-CoA synthetase enzymes. As protein expression of ACSS2 was markedly increased in *ACLY*-KO cells (Fig. 1B, S1A), we hypothesized that acetate utilization may compensate for loss of ACLY. Supplementation of 1 mM [1,2-$^{13}C_2$] acetate to cultures rescued palmitate synthesis in cells lacking ACLY (Fig. 2A, S2A). Acetate became the primary lipogenic substrate in all tested *ACLY*-KO cell lines (Fig. 2B, S2B) but only contributed between 5-40% of lipogenic acetyl-CoA pools in control cells. *De novo* palmitate synthesis was rescued in the *ACLY*-KO cells grown with acetate (Fig. 2A, S2A) compared to those grown in the absence of acetate (Fig. 1F, S1F,G) in all cell lines. We also measured the growth rate of control and ACLY-deficient cell lines in various culture media. *ACLY*-KO cells grew comparably to control cells in media supplemented with 10% dialyzed fetal bovine serum (dFBS) (Fig 2C, S2C); however, when we removed serum lipids growth of all *ACLY*-KO cells was severely compromised (Fig 2C, S2C). Addition of 1 mM exogenous acetate enhanced the growth of all *ACLY*-KO cell lines while having no impact on growth rates of control cells (Fig 2C, S2C). The most dramatic growth impact of acetate was observed in cultures grown in delipidated serum (Fig 2C, S2C), highlighting the importance of this metabolic redundancy in supporting acetyl-CoA for lipid synthesis (Fig. 2D).

To confirm the role of ACSS2 in supporting lipogenesis, we examined the growth and metabolism of A549 and HepG2 cells lacking ACSS2 (Fig. 3A, S3A). While ACLY expression was unchanged in *ACSS2*-KO cells (Fig. 3A, S3A), the conversion of [1,2-$^{13}C_2$]acetate to palmitate was significantly decreased (Fig. 3B, S3B), and there was no impact on palmitate synthesis rates in cells lacking ACSS2 (Fig. 3C, S3C). Furthermore, the growth rates of both A549 and HepG2 cell lines were minimally impacted by *ACSS2*-KO in lipid-replete medium (Fig. 3D, S3D). However, HepG2 ACSS2-KO cells observed a significant growth defect compared to wildtype in lipid-depleted media (Fig S3D), matching previous studies which found ACSS2-KD was detrimental to cancer cell growth in conditions of metabolic stress (*31*, *34*). A549 ACSS2-KO cell growth remained unaffected by media delipidation (Fig. 3D). A similar phenotype bifurcation between the cell lines was observed previously, as HepG2 cells exhibited a greater growth rate reduction upon loss of ACLY compared to A549 cells (Fig. 1C, S1B). Interestingly, mRNA expression of ACSS1 and ACSS3, both mitochondrial isozymes of ACSS2, were significantly elevated in HepG2 hepatocarcinoma cells compared to A549 NSCLC cells (Fig. 3E). Furthermore, [1,2-$^{13}C_2$]acetate enrichment of TCA intermediates was substantially higher in HepG2 cells compared to A549 cells (Fig. 3F,G), suggesting that mitochondrial ACSS1 and/or ACSS3 compete with cytosolic ACSS2 for utilization of acetate and likely reflecting the metabolism in their tissues of origin. This metabolic redundancy may influence acetate shuttling to mitochondria, lipid pathways (e.g. ER),

and nucleus to impact epigenetic regulation which is altered by ACSS1/2 knockdown (*45*) but also suggests this pathway may not be targetable in all tumor or cell types.

Alternative pathways compensate for combined loss of ACLY and ACSS2

Next we characterized A549 ACLY/ACSS2 double knockout (*ACLY/ACSS2*-DKO) cells to explore how cancer cells respond to extreme restriction of acetyl-CoA sourcing (Fig. 4A). As expected, growth of A549 *ACLY/ACSS2*-DKO cells was significantly impaired relative to wildtype in all conditions tested, and we observed no rescue-effect with acetate supplementation (Fig 4B). We also detected little to no isotope enrichment in palmitate from [U-$^{13}C_6$]glucose or [1,2-$^{13}C_2$]acetate in *ACLY/ACSS2*-DKO cells (Fig. 4C, D), confirming that both pathways were defective in these cells. Mammalian cells do not synthesize polyunsaturated fatty acids (PUFAs) *de novo* and instead rely on exogenous sources. Incorporation of PUFAs into phosphatidylcholine (PC) and triacylglycerols (TAGs) is elevated in *ACLY* and *ACLY/ACSS2* DKO cells, indicating increased contribution of exogeneous fatty acids in membrane lipids in *ACLY* deficient cells (Fig. 4E, S4A, B). To further confirm this change in lipids in ACLY deficient cells we examined their sensitivity to ferroptosis. PUFA-containing lipids readily undergo peroxidation (*46*), and we found that PUFA-enriched *ACLY/ACSS2*-DKO cells were more susceptible to ferroptosis induced by application of the glutathione peroxidase 4 (GPX4) inhibitor, ML210, compared to wildtype cells (Fig. 4F). Despite these alterations in lipid metabolism, acetylated histone acH3K27 (Fig. 4G) and whole cell protein acetylation was maintained in lipid-replete *ACLY*-KO and *ACLY/ACSS2*-DKO cells (Fig S4C, D), suggesting that NSCLC cells can sustain acetyl-CoA availability through pathways independent of ACLY and ACSS2.

The continued availability of acetyl-CoA for histone acetylation suggests cancer cells can employ alternate pathways for acetyl-CoA generation under conditions of metabolic stress, including non-enzymatic mechanisms (*47*). To explore these pathways more deeply we cultured A549 *ACLY*-KO and *ACLY/ACSS2*-DKO cells with either ^{13}C-labeled glucose, glutamine, and pyruvate for 72 hours and quantified isotope enrichment in palmitate. In theory, knockout of ACLY will eliminate glucose to palmitate carbon transfer (Fig. 5A); however, A549 *ACLY*-KO cells traced with [U-$^{13}C_6$]glucose continued to sustain labeling on newly synthesized palmitate (Fig. 5B), and we observed similar results with [3-^{13}C]pyruvate (Fig. 5C). Culture of the *ACLY*-KO and *ACLY/ACSS2*-DKO cells with [U-$^{13}C_5$]glutamine yielded insignificant enrichment of palmitate (Fig. 5D), and this pathway was inactive even under hypoxia, where glutamine contributed little to fatty acid synthesis in *ACLY*-KO cells (Fig. S5G). These data suggest the existence of a citrate/ACLY-independent lipogenic pathway which allows glucose and pyruvate but not glutamine to generate acetyl-CoA. We previously demonstrated that carnitine acetyl-transferase (CRAT) actively exports mitochondrial branched-chain-CoAs to enable their elongation to long-chain monomethyl branched-chain fatty acids in adipocytes (*48*), and Izzo et al. have observed that CRAT facilitates nuclear acetylation and lipogenesis in hepatocellular carcinoma cells (*49*). However, we observed minimal labeling of palmitate from [U-$^{13}C_6$]glucose in the A549 *ACLY/ACSS2*-DKO (Fig. 5B), despite noting significant enrichment of citrate (Fig. S5B). To investigate whether mitochondrial metabolism was required for conversion of glucose carbon to lipids in *ACLY*-KOs, we treated cells with the mitochondrial pyruvate carrier (MPC) inhibitor UK5099. MPC treatment significantly decreased fatty acid synthesis and lipogenic acetyl-CoA labeling in A549 wild type (WT) cells (Fig. S5E-F), but we observed no effect in *ACLY*-KO cells. Moreover, MPC inhibition increased the relative contribution of glucose to palmitate-directed acetyl-CoA (Fig. S5E-F), further suggesting that mitochondrial pyruvate metabolism is not contributing significantly to palmitate synthesis in these *ACLY*-KO A549 cells. Likewise, ^{13}C pyruvate, and glutamine also yielded negligible label on palmitate in A549 *ACLY/ACSS2*-DKO cells (Fig. 5B, C, D), suggesting that ACSS2 is involved in the conversion of pyruvate to acetyl-

CoA (Fig. 5A). Such a mechanism has been described whereby reactive oxygen species facilitate oxidative decarboxylation of pyruvate to acetate (*50*). The combination of KO cells and tracers applied here suggest this activity supports acetyl-CoA generation, but the extracellular acetate, ACSS2, and lipid dependency of *ACLY*-KO cell growth suggests this *de novo* acetate flux is not significant enough to sustain the biosynthetic needs of the ACLY deficient cells tested here (Fig. 2C, S2C).

To examine how oxidation of fatty acyl-CoA might contribute to acetyl-CoA homeostasis we traced the A549 cell panel with 500 μM [U-$^{13}C_8$]octanoate, which passively diffuses across the mitochondrial membrane as well as peroxisomal membranes (*39*). Notably, octanoate contributed significantly to fatty acid biosynthesis, even in *ACLY/ACSS2*-DKO cells (Fig. 5E,F, S5C) and contrasting results with glucose, acetate, or glutamine tracers (Fig 4C, D, 5D). *ACLY*-KO and *ACLY/ACSS2*-DKO cells had a 2.5-fold and 4-fold increase, respectively, in enrichment of the lipogenic acetyl-CoA pool from octanoate compared to the wildtype or *ACSS2*-KO cells (Fig. 5E). Similar trends in lipogenic acetyl-CoA labeling from [U-$^{13}C_8$]octanoate were observed in HepG2 and 634T *ACLY*-KO clones (Fig. S5C). Indeed, supplementation of octanoate enabled quantitation of fractional new fatty acid synthesis in *ACLY/ACSS2*-DKO cells by ISA (Fig. 5F). Citrate enrichment from octanoate was also increased in the *ACLY*-KO and *ACLY/ACSS2*-DKO cells (Fig. S5D). However, based on the previous [U-$^{13}C_5$]glutamine tracing results (Fig. 5D) mitochondrial citrate minimally contributes to fatty acid synthesis in the *ACLY*-KO or *ACLY/ACSS2*-DKO cells, and no carnitine was added to cultures(*49*), suggesting that ACLY-deficient cells use peroxisomal metabolism to supply acetyl-CoA for biosynthesis (Fig 5G).

Peroxisomal β-oxidation supplies lipogenic acetyl-CoA in the absence of ACLY and ACSS2

Peroxisomes are the site of β-oxidation for VLCFAs and BCFAs. Peroxisomes are closely associated with lipid droplets and contain the metabolic machinery for acetyl-CoA generation from diverse fatty acids (*51*). In fact, Izzo et al. observed increased expression of peroxisomal fatty acid oxidation genes in their *ACLY/ACSS2*-DKO cell lines (*49*). To test whether peroxisomes could serve as an appreciable source of acetyl-CoA in cancer cells, we profiled lipid abundances in the A549 cell panel. While total TAGs were slightly reduced in most cells, total PCs were unchanged (Fig. 6A). However, we detected significant alterations in the acyl-chain composition of the lipids, such that TAGs and PCs containing VLCFAs were depleted in *ACLY*-KO and *ACLY/ACSS2*-DKO cells (Fig. 6B, C). This depletion is complete for nearly all measurable VLCFA containing saturated, mono-, and di-unsaturated TAG species (Fig. S6A) as well as saturated, and mono-unsaturated PC species (Fig S6B). Depletion of VLCFAs in lipids suggests altered VLCFA homeostasis, potentially due to increased VLCFA oxidation in the peroxisome or decreased elongation using acetyl-CoA.

To further investigate we studied role of peroxisomes in non-canonical lipogenic acetyl-CoA contribution. Peroxisome maintenance depends on the import of nuclear-encoded proteins containing a peroxisomal targeting signals (PTS1), which are recognized by cytosolic PEX5 receptors that transport them into the peroxisomal lumen. In the absence of PEX5 peroxisomal enzyme transport is ablated and metabolism altered (*52*). To further investigate the role of peroxisomes in supporting acetyl-CoA metabolism we generated *PEX5* and *ACLY/PEX5*-knockout (*ACLY/PEX5*-KO) clones using CRISPR/Cas9 in A549 cells (Fig. 6D). *ACLY/ACSS2/PEX5* triple knockout cells did not proliferate and could not be tested. We then cultured A549 *PEX5*-KO cells with 500 μM [U-$^{13}C_8$]octanoate and quantified its contribution to the lipogenic acetyl-CoA pool. Intriguingly, both enrichment from octanoate and fatty acid synthesis were significantly lower in *ACLY/PEX5*-KO cells compared to *ACLY*-KO cells (Fig 6E-F), providing evidence that peroxisomal metabolism supports acetyl-CoA and lipid synthesis. On the other hand, we saw no

291 effect of PEX5 deficiency on lipogenic acetyl-CoA enrichment or palmitate synthesis in wildtype
292 cells (Fig 6E-F). The labeling distribution of palmitate from [U-$^{13}C_8$]octanoate highlights these
293 changes, as *ACLY*-KO cells showed robust incorporation but *ACLY/PEX5*-KO cells showing
294 predominantly M8 palmitate (or direct incorporation of octanoate; Fig. S6C). These data suggest
295 that knockout of PEX5 disrupts the contribution of peroxisomal fatty acid oxidation to lipogenic
296 acetyl-CoA production in the ACLY-KO cells (Fig 6G). In fact, we also observed a decrease in
297 octanoate-mediated histone acetylation in *ACLY*/*PEX*5-KOs compared to *ACLY*-KO cells in
298 delipidated media (Fig. S6D). To further support peroxisomal oxidation in *ACLY*-KO cells we
299 traced with long chain fatty acid [U-$^{13}C_{18}$] oleate (38). We observed an increase in
300 lysophosphatidylcholine (LPC) 16:1 enrichment from [U-$^{13}C_{18}$]oleate in *ACLY* KO cells compared
301 to WT A549 cells, indicating increased reliance on exogenous fatty acid oxidation (Fig. 6H). As
302 expected in *ACLY/PEX*5 KOs LPC 16:1 enrichment from [U-$^{13}C_{18}$]oleate decreased (Fig. 6H).
303
304 To elucidate how impairing peroxisomal β-oxidation affects proliferation of cells lacking ACLY,
305 we quantified the growth of each cell line in response to knockout of *PEX5*. Strikingly,
306 *ACLY/PEX5*-KO cells showed a significant decrease in growth relative to *ACLY*-KO cells, whereas
307 there was no growth effect on single *PEX5*-KO cells compared to wildtype (Fig. 6I). Finally, we
308 quantified the growth of entire A549 ACLY/ACSS2-KO cell panel in response to increasing
309 concentrations of the peroxisomal β-oxidation inhibitor, Thioridazine (Thio) (*53*, *54*). Strikingly,
310 *ACLY*-KO and *ACLY/ACSS2*-DKO cells were significantly more sensitive to Thio treatment than
311 wildtype or *ACSS2*-KO cells (Fig S6E). Application of 2.5 μM Thio had no appreciable impact on
312 growth of wildtype and *ACSS2*-KO cells, but significantly decreased proliferation of *ACLY*-KO and
313 *ACLY/ACSS2*-DKO cells (Fig. 6J). Together, these results suggest that peroxisomal β-oxidation
314 provides a significant growth sustaining level of acetyl-CoA in the absence of functional ACLY.
315 Multiple mechanisms have been suggested for shuttling peroxisomal acetyl-CoA to the cytosol in
316 mammalian cells, including conversion to acetate by a thioesterase and subsequent export (and
317 activation by ACSS2 in the cytosol), shuttling as acetyl-carnitine facilitated by peroxisomal CRAT
318 (*55–57*) or via peroxisomal coenzyme A transporters like solute carrier family 25 member 17
319 (Slc25a17) and ATP binding cassette subfamily D member 1 (ABCD1) (*58–60*). To this end, we
320 observed a significant increase in acetyl-carnitine enrichment from [U-$^{13}C_8$]octanoate in *ACLY*-KO
321 and *ACLY/ACSS2*-DKO cells compared to WT cells (Fig. S6F), cells that are both capable of (and
322 actually prefer) synthesizing palmitate from [U-$^{13}C_8$]octanoate (Fig. 5E). Furthermore, acetyl-
323 carnitine enrichment from octanoate was significantly decreased in *ACLY/PEX5*-KOs (Fig. S6G),
324 providing evidence that peroxisomal metabolism supports acetyl-CoA and lipid synthesis in the
325 absence of ACLY. Altogether, these metabolic tracing and knock out studies emphasize that
326 peroxisomal oxidation of exogenous lipids as a major source of acetyl-CoA for fatty acid synthesis
327 and histone acetylation in ACLY-deficient cells, highlighting a role for inter-organelle crosstalk in
328 supporting cell survival in response to nutrient fluctuations.
329
330 **Discussion**
331
332 While the core metabolic machinery of cancer cells acts "as advertised" under nutrient replete
333 conditions, the diverse stresses experienced the tumor microenvironment induce complex rewiring
334 of metabolic fluxes between organelles, including mitochondria, the ER, peroxisomes, and the
335 plasma membrane. Here we show this organelle crosstalk is critical for cancer cells to maintain
336 acetyl-CoA homeostasis and metabolic resilience when organelle-specific pathways become
337 compromised. Acetyl-CoA serves as a substrate regulating numerous processes across
338 mitochondria, the nucleus, peroxisomes, the ER, and plasma membrane but importantly cannot
339 cross membranes. As such, understanding how acetyl-groups are shuttled throughout the cell for
340 bioenergetics, biosynthesis, and cellular regulation is critically important. Here we applied

metabolic tracing and lipogenesis studies to cancer cell lines where key pathways for acetyl-CoA generation were knocked out, including ACLY, ACSS2, and peroxisomal metabolism (PEX5). We further highlight a key role for peroxisomal metabolism in providing acetyl-CoA for fatty acid synthesis and histone acetylation in the context of ACLY deficiency.

Acetyl-CoA-fueled fatty acid synthesis is important for cancer progression in NSCLC models, whether this occurs in endogenous tissues or in situ within tumors (*7*). Targeting of ACLY to reduce tumor cell growth and increase dependence on exogenous lipids has also been explored in detail (*24–26*, *61*). Likewise, ACSS2 has garnered significant interest as a mechanism through which cancer cells source acetyl-CoA for growth and survival (*31–33*, *62*). ACSS2 expression and acetate-dependent flux both increase in the context of ACLY deficiency (*36*), and trafficking of acetate to the nucleus for histone acetylation may be an important aspect of this enzyme's function (*45*, *63–65*). The impact of ACSS isozyme expression on acetate shuttling, fatty acid synthesis and epigenetic regulation warrants further study as it may provide insight into how therapeutic interventions targeting acetate catabolism impact whole body physiology. Peroxisomes further complicate these questions, particularly in reference to their impact on lipid homeostasis and diversity. Understanding how these nodes of metabolic exchange are exploited by cancer cells shed light on resistance mechanisms, as these redundancies in pathway architecture can reduce efficacy of drugs targeting metabolic enzymes (*66*).

Beyond cancer, understanding how cells manage intracellular metabolic pools using these KO and tracing approaches is also relevant for states of "overnutrition." Indeed, exogenous treatment of fatty acids or lipids to cells in vitro often occurs at supra-physiological levels, so our studies further highlight the role of peroxisomal metabolism in generating acetyl-CoA for lipid biosynthesis and acetylation (*51*). While these KO systems lack some physiology in the acute nature of pathway targeting, they also allow one to focus biochemical studies on these alternate pathways when substrate levels are high. However, we and Izzo et al(*49*). in this issue also note key questions that remain such as the relative contribution of mitochondrial versus peroxisomal oxidation and the dependence on carnitine for transport since both organelles express CRAT (*67*, *68*). Our data indicate that the mitochondrial pathway is not sufficiently active to support cell growth in these cells, suggesting a role for peroxisomes in some cells or environments where carbohydrates are deficient or mitochondria inactive (e.g. hypoxia). Importantly, the relative contribution of each pathway likely shifts as a function of cell and tissue type. By understanding how these metabolic pathways are balanced they can be more effectively targeted both in neoplastic or metabolically stressed tissues.

Materials and Methods

Cell Lines

A549 and HepG2 cells were obtained from HDBiosciences, HAP1 cells were obtained from Horizon Discovery, and 634T cells were obtained from the Shaw Lab at the Salk Institute for Biological Sciences. All cell lines were incubated at 37C with 5% CO_2 and cultured using Dulbecco's Modified Eagle Media (DMEM) with 10% Fetal Bovine Serum and 1% Penicillin-Streptomycin. Cells tested negative for mycoplasma contamination. All media were adjusted to pH = 7.3.

Cell Proliferation and ^{13}C Tracing

Proliferation studies were performed on 12 well plates with an initial cell number of 50,000/well for A549s and 100,000/well for HepG2s. Cells were plated in growth media and allowed to adhere

for 24 hours before changing to the specified growth media. Cell counts were performed at days 0 and 4 using a hemocytometer.

^{13}C isotope tracing media was formulated using glucose and glutamine free DMEM 5030 supplemented with either 20 mM [U-$^{13}C_6$]glucose, 4 mM [U-$^{13}C_5$]glutamine, 1 mM [1,2-$^{13}C_2$]acetate, 5 mM [3-$^{13}C_1$]pyruvate, 500 µM [U-$^{13}C_8$] octanoate or 500 µM [2,4-$^{13}C_2$]citrate, (Cambridge Isotopes) and 10% dialyzed FBS. ^{13}C oleate studies were performed with 100 µM albumin conjugated [U-$^{13}C_{18}$] oleate and 10% dialyzed FBS. All studies were performed with a final concentration of 20 mM glucose and 4 mM glutamine. Cultured cells were washed with 1 mL PBS prior to applying tracing media for 6-72 hours as indicated in figure legends.

Drug Dose Response

Drug dose response studies were performed on 96 well plates with an initial cell number of 2,500/well. Cells were plated in growth media and allowed to adhere for 24 hours before changing to the specified growth media with the indicated concentration of thioridazine. After 4 days wells were washed 2x with tap water, 50uL of 0.5% crystal violet staining solution were added to each well for 20 minutes. Crystal violet stain was removed, and wells were washed 3x with tap water and air dried overnight. Next, 200 uL methanol was added to each well and plates were incubated at room temperature for 20 minutes. Optical density of wells was measured at 570 nm on a TECAN plate reader.

Ferroptosis Assay

Wildtype and ACLY/ACSS2-DKO cells were plated in 96 well plates with an initial cell number of 5,000/well. Cells were plated in growth media and allowed to adhere for 24 hours before changing to the specified growth media with 2uM ML210 and/or 6uM Ferrostatin. After 48 hours, cell viability was quantified using the PrestoBlue™ Cell Viability (Thermo, A13261) and a TECAN plate reader.

Isotopomer Spectral Analysis (ISA)

Isotopomer spectral analysis (ISA) was performed to estimate the percent of newly synthesized palmitate as well as the contribution of a tracer of interest to the lipogenic acetyl-CoA pool (*69*, *70*). Parameters for contribution of ^{13}C tracers to lipogenic acetyl-CoA (D value) and percentage of newly synthesized fatty acid (g(t) value) and their 95% confidence intervals are then calculated using best-fit model from INCA MFA software. Experimental palmitate labeling from [U-$^{13}C_6$]glucose, [U-$^{13}C_5$]glutamine, [1,2-$^{13}C_2$]acetate, [U-$^{13}C_8$] octanoate or [2,4-$^{13}C_2$]citrate after a 24-72 hour trace, as indicated in figure legends, was compared to simulated labeling using a reaction network where C16:0 is condensation of 8 AcCoA. ISA data plotted as mean ± 95% CI. * indicates statistical significance by non-overlapping confidence intervals. Reaction model and the fragment ion(s) of palmitate used in the ISA method are included in supplementary table S2.

CRISPR/cas9 engineered knockout cell lines

HDBiosciences generated A549 and HepG2 *ACLY*-KO, *ACSS2*-KO, and *ACLY/ACSS2*-DKO cell lines. *ACLY, ACSS2,* and *ACLY/ACSS2* knockout clones were generated using the strategy described previously (*71*). Briefly, a tandem guide RNAs (gRNAs) was designed to target the human *ACLY* (gRNA sequences: gaccagctgatcaaacgtcg, ggggtcaggatgaacgtgtg) and *ACSS2* (gRNA sequences: ctcgcggtagcgctgcagcg, aatggaaaagggattccggg) using the online CRISPR guide tool provided by the Zhang Lab at MIT (https://zlab.bio/guide-design-resources). The gRNA duplex was cloned into lentiCRISPRv2 (Addgene #52961) (*72*). A549 and HepG2 cells were transfected with the *ACLY* and/or *ACSS2* specific gRNA to generate pooled knockouts. After puromycin selection, single-cell clones were isolated by diluting the pooled knockout lines at 1 cell/100 µL

and plating 100 µL into each well of a 96 well plate. Clones were maintained by exchanging media every 3-5 days. Clones were validated by PCR and western blot. PEX5 and ACLY/PEX5 knockout clones were generated using the strategy described previously (*73*). Briefly, chemically modified guide RNAs (gRNAs) (Synthego) were designed to target the human PEX5 (gRNA sequences: guugguggcugaauucc). gRNAs were complexed with recombinant Cas9 (IDT Cat#1081059) and introduced into cells by electroporation (4D-Nucleofector, Lonza Biosciences) according to manufacturer protocols. Single cell clones were generated by serial dilution of the bulk knockout population in 96 well plates. Clones were maintained by exchanging the media every 3 days and validated by western blot.

Lentivirus Production

One 10cm dish of HEK293FT cells at 60% confluency were transfected with 1.3 µg VSV.G/pMD2.G, 5.3 µg lenti-gag/pol/pCMVR8.2, and 4 µg of the gRNA duplexed lentiCRISPRv2 using 16 µL Lipofectamine 3000 diluted in 0.66 mL of OPTI-MEM. Medium containing viral particles was harvested 48 and 72 hours after transfection, then concentrated by Centricon Plus-20 100,000 NMWL centrifugal ultrafilters, divided into aliquots and frozen at -80°C.

Metabolic Flux Analysis

Metabolic fluxes for citrate were calculated by collecting media at time 0 and spent media after 72 hours. Spent media was centrifuged at 300g for 5 min, to remove cell debris. Cell counts were performed at time 0 and after 72 hours as well.

Metabolite Extraction and GC-MS Analysis

At the conclusion of the tracer experiment, media was aspirated. Then, cells were rinsed twice with 0.9% saline solution and lysed with 250 µL ice-cold methanol. After 1 minute, 100 µL water containing 1 µg/ml norvaline was added to each sample and vortexed for one minute. 250 µL chloroform was added to each sample, and all were vortexed again for 1 minute. After centrifugation at 21,130 g for 10 minutes at 4°C, 250 µL of the upper aqueous layer was collected and evaporated under vacuum at 4°C. Then, 250 µL of the lower organic layer was collected and evaporated under air at room temperature. Dried polar and nonpolar metabolites were processed for gas chromatography (GC) mass spectrometry (MS) as described previously in Cordes and Metallo (*70*). Briefly, polar metabolites were derivatized using a Gerstel MultiPurpose Sampler (MPS 2XL). Methoxime-tBDMS derivatives were formed by addition of 15 µL 2% (w/v) methoxylamine hydrochloride (MP Biomedicals, Solon, OH) in pyridine and incubated at 45°C for 60 minutes. Samples were then silylated by addition of 15 µL of N-tert-butyldimethylsily-N-methyltrifluoroacetamide (MTBSTFA) with 1% tert-butyldimethylchlorosilane (tBDMS) (Regis Technologies, Morton Grove, IL) and incubated at 45°C for 30 minutes. Nonpolar metabolites were saponified and transesterified to fatty acid methyl esters (FAMEs) by adding 500 µL of 2% H_2SO_4 in methanol to the dried nonpolar layer and heating at 50°C for 1 hour. FAMEs were then extracted by adding 100 µL of a saturated salt solution and 500 µL hexane and vortexing for 1 minute. The hexane layer was removed, evaporated, and resuspended with 60µL hexane for injection.

Derivatized polar samples were injected into a GC-MS using a DB-35MS column (30m x 0.25mm i.d. x 0.25µm, Agilent J&W Scientific, Santa Clara, CA) installed in an Agilent 7890B GC system integrated with an Agilent 5977a MS. Samples were injected at a GC oven temperature of 100°C which was held for 1 minute before ramping to 255°C at 3.5°C/min then to 320°C at 15°C/min and held for 3 minutes. Electron impact ionization was performed with the MS scanning over the range of 100-650 m/z for polar metabolites.

490 Derivatized nonpolar samples were injected into a GC-MS using a Fame Select column (100m x
491 0.25mm i.d. x 0.25µm, Agilent J&W Scientific, Santa Clara, CA) installed in an Agilent 7890A GC
492 system integrated with an Agilent 5977A MS. Samples were injected at a GC oven temperature of
493 80°C which was held for 1 minute before ramping to 170°C at 20°C/min then to 188°C at 1°C/min
494 then to 250°C at 20°C/min and held for 10 minutes. Electron impact ionization was performed with
495 the MS scanning over the range of 54-400 m/z for nonpolar metabolites.
496 Metabolite levels and mass isotopomer distributions were analyzed with an in-house Matlab script
497 which integrated the metabolite fragment ions and corrected for natural isotope abundances. Mole
498 percent enrichment calculations were performed using Escher-Trace (*74*).
499
500 **LC-MS/MS analysis**
501 Lipids were extracted from confluent 6 well plates after growth in DMEM + 10% FBS + 1%
502 penicillin streptomycin for 48 hours. At the conclusion of the experiment, media was aspirated, and
503 the cells were rinsed twice with saline solution. Cells were lysed with 750 µL of ice cold 1:1
504 methanol/water solution for 5 minutes on ice and scraped into Eppendorf tubes. Next, 500 µL of
505 ice cold chloroform and 50 uL butylated hydroxytoluene (1mg/mL in methanol) were added to the
506 tube, along with EquiSLASH (Avanti, Croda International Plc, 330731internal standard. The tubes
507 were vortexed for 5 min and centrifuged at 21,230g at 4°C for 5 min. The lower organic phase was
508 collected and 2 µL of formic acid was added to the remaining polar phase which was re-extracted
509 with 500uL of chloroform. Combined organic phases were dried under nitrogen and the pellet was
510 resuspended in 50 µL isopropyl alcohol.
511
512 Q Exactive orbitrap mass spectrometer with a Vanquish Flex Binary UHPLC system (Thermo
513 Scientific) was used with an Accucore C30, 150 x 2.1mm, 2.6 µm particle (Thermo) column at
514 40°C. 5 µL of sample was injected. Chromatography was performed using a gradient of 40:60 v/v
515 water: acetonitrile with 10 mM ammonium formate and 0.1% formic acid (mobile phase A) and
516 10:90 v/v acetonitrile: 2-propanol with 10 mM ammonium formate and 0.1% formic acid (mobile
517 phase B), both at a flow rate of 0.2 mL/min. The LC gradient ran from 30% to 43% B from 3-8
518 min, then from 43% to 50% B from 8-9min, then 50-90% B from 9-18min, then 90-99% B from
519 18-26 min, then held at 99% B from 26-30min, before returning to 30% B in 6 min and held for a
520 further 4 min.
521
522 Lipids were analyzed in positive mode using spray voltage 3.2 kV. Sweep gas flow was 1 arbitrary
523 units, auxiliary gas flow 2 arbitrary units and sheath gas flow 40 arbitrary units, with a capillary
524 temperature of 325°C. Full MS (scan range 200-2000 m/z) was used at 70 000 resolution with 1e6
525 automatic gain control and a maximum injection time of 100 ms. Data dependent MS2 (Top 6)
526 mode at 17 500 resolution with automatic gain control set at 1e5 with a maximum injection time of
527 50 ms was used. Data was analyzed using EI-Maven and Escher-Trace software, and peaks
528 normalized to Avanti EquiSPLASH internal standard. Lipid species specific fragments used for
529 identification and quantitation are presented in the Supplementary Table 1
530

531 For acetyl carnitine measurement polar phase was dried under air and the pellet was resuspended
532 in 50 µL acetonitrile and loaded on to Q Exactive orbitrap mass spectrometer with a Vanquish
533 Flex Binary UHPLC system (Thermo Scientific) was used with an iHILIC - (P) Classic, 150 x
534 2.1mm, 5 µm particle, 200 Å (Hilicon) column at 45°C. 5 µL of sample was injected.
535 Chromatography was performed using a gradient of 20 mM ammonium carbonate, adjusted to pH
536 9.4 with 0.1% ammonium hydroxide (25%) solution (mobile phase A) and 100% acetonitrile
537 (mobile phase B), both at a flow rate of 0.2 mL/min. The LC gradient ran linearly from 80% to
538 20% B from 2-17 min, then from 20% to 80% B from 17-18 min, then held at 80% B from 18-25
539 min.

540
541 **Western Blot**
542 A549, HepG2, HAP1, and 634T wildtype, ACLY and/or ACSS2-KO cell lines were lysed in M-
543 PER buffer (Thermo Scientific, 78501) with 1x protease inhibitor (Sigma-Aldrich). Protein
544 concentrations were determined using Pierce™ BCA protein assay kit (Thermo Scientific, 23225).
545 15 ug protein were loaded and separated using 4–15% Mini-PROTEAN® TGX™ Precast SDS-
546 PAGE Gels (Bio-rad, #4561086). Samples were then transferred to nitrocellulose membranes for
547 immunoblotting. Total acetylated-lysine (Cell Signaling Technology, 9441), β-Actin (Sigma,
548 A5441), ACLY (Cell Signaling Technology, 13390), and ACSS2 (Cell Signaling Technology,
549 3658), PEX5(D7V4D) (Cell Signaling Technology, 83020) antibodies were used to probe their
550 respective targets. Anti-Rabbit horseradish peroxidase-conjugated secondary antibodies (Millipore,
551 AP132P) were used for imaging.
552
553
554 **Acid Extraction of Histones**
555 Cells were washed with ice cold PBS and lysed with NIB-250 buffer (15 mM Tris-HCl (pH 7.5),
556 5 mM MgCl2, 15 mM NaCl, 60 mM KCl, 1mM CaCl2, 1 mM DTT, 250 mM sucrose, 10 mM
557 sodium butyrate, protease inhibitors) with 0.1% NP-40 incubate on ice for 5 minutes. Nuclei were
558 pelleted at 600g for 5 min at 4°C. Wash nuclei pellet gently with 150 uL NIB-250 without NP-40.
559 Resuspend the extracted nuclei with 0.4N H_2SO_4 and rotate for 4 hours or overnight at 4°C to
560 extract histone proteins, then centrifugation at 11,000g at 4°C for 10 minutes. To the Clarified
561 histone extracts slowly add 100% TCA to final concentration of 20%. Let this mixture precipitate
562 on ice for at least 1 hour or as long as overnight. Precipitated histones were centrifuged at 11,000g
563 at 4°C for 10 minutes. Histones were washed with 1 mL acetone + 0.1% 12 N HCl once and 1 mL
564 acetone twice. The histone pellet was air dried at room temperature then resuspended in glass
565 distilled H2O. Resuspended histones were used for western blotting.
566
567
568 **RNA isolation and quantitative RT-PCR**
569 Total RNA was purified from cultured cells using Trizol Reagent (Life Technologies) per
570 manufacturer's instructions. First-strand cDNA was synthesized from 1 µg of total RNA using
571 iScript Reverse Transcription Supermix for RT-PCR (Bio-Rad Laboratories) according to the
572 manufacturer's instructions. Individual 20 µl SYBR Green real-time PCR reactions consisted of 1
573 µl of diluted cDNA, 10 µl of SYBR Green Supermix (Bio-Rad), and 1 µl of each 5 µM forward
574 and reverse primers. For standardization of quantification, 18S was amplified simultaneously. The
575 PCR was carried out on 96-well plates on a CFX Connect Real time System (Bio-Rad), using a
576 three-stage program provided by the manufacturer: 95 °C for 3 min, 40 cycles of 95 °C for 10 s
577 and 60 °C for 30 s. Gene-specific primers are tabulated in Table S1.
578
579 **Quantification and Statistical Analysis**
580 Statistical analyses were performed using Graphpad PRISM. Unless indicated, all results shown as
581 mean ± SD of cellular triplicates obtained from one representative experiment as specified in each
582 figure legend. P values were calculated using a Student's two-tailed *t* test, One-way ANOVA w/
583 Dunnet's method for multiple comparisons, or Two-way ANOVA w/ Tukey's method for multiple
584 comparisons; *, P value < 0.05; **, P value < 0.01; ***, P value < 0.001, ****, P value < 0.0001.
585 Unless indicated, all normalization and statistical tests compared to wildtype cells.
586
587
588

589 **References**

590

591 1. J. A. Menendez, R. Lupu, Fatty acid synthase and the lipogenic phenotype in cancer
592 pathogenesis. *Nat. Rev. Cancer*. **7** (2007), doi:10.1038/nrc2222.
593 2. Y. Cai, J. Crowther, T. Pastor, J. Dehairs, J. V Swinnen, A. A. Sablina, Loss of
594 Chromosome 8p Governs Tumor Progression and Drug Response by Altering Lipid
595 Metabolism Article Loss of Chromosome 8p Governs Tumor Progression and Drug
596 Response by Altering Lipid Metabolism. *Cancer Cell*. **29**, 751–766 (2016).
597 3. M. Knobloch, S. M. G. Braun, L. Zurkirchen, C. Von Schoultz, N. Zamboni, M. J. Arauzo-
598 bravo, W. J. Kovacs, Ö. Karalay, R. A. C. Machado, M. Roccio, M. P. Lutolf, C. F.
599 Semenkovich, S. Jessberger, Metabolic control of adult neural stem cell activity by Fasn-
600 dependent lipogenesis. *Nature*. **493**, 226–230 (2014).
601 4. T. M. Loftus, D. E. Jaworsky, G. L. Frehywot, C. A. Townsend, G. V Ronnett, M. D. Lane,
602 F. P. Kuhajda, Reduced Food Intake and Body Weight in Mice Treated with Fatty Acid
603 Synthase Inhibitors. *Science (80-.).* **288**, 2379–2382 (2000).
604 5. J. A. Menendez, L. Vellon, I. Mehmi, B. P. Oza, S. Ropero, R. Colomer, R. Lupu,
605 Inhibition of fatty acid synthase (FAS) suppresses HER2/neu (erbB-2) oncogene
606 overexpression in cancer cells. *Proc. Natl. Acad. Sci.* **101**, 10715–10720 (2004).
607 6. E. S. Pizer, J. Thupari, W. F. Han, M. L. Pinn, F. J. Chrest, G. L. Frehywot, C. A.
608 Townsend, F. P. Kuhajda, Malonyl-Coenzyme-A Is a Potential Mediator of Cytotoxicity
609 Induced by Fatty-Acid Synthase Inhibition in Human Breast Cancer Cells and Xenografts
610 1. *Cancer Res.* **60**, 213–218 (2000).
611 7. R. U. Svensson, S. J. Parker, L. J. Eichner, M. J. Kolar, M. Wallace, S. N. Brun, P. S.
612 Lombardo, J. L. Van Nostrand, A. Hutchins, L. Vera, L. Gerken, J. Greenwood, S. Bhat, G.
613 Harriman, W. F. Westlin, H. J. Harwood, A. Saghatelian, R. Kapeller, C. M. Metallo, R. J.
614 Shaw, Inhibition of acetyl-CoA carboxylase suppresses fatty acid synthesis and tumor
615 growth of non-small-cell lung cancer in preclinical models. *Nat. Med.* **22**, 1108–1119
616 (2016).
617 8. K. E. Wellen, G. Hatzivassiliou, U. M. Sachdeva, T. V Bui, J. R. Cross, C. B. Thompson,
618 ATP-Citrate Lyase Links Cellular Metabolism to Histone Acetylation. *Science (80-.).* **324**,
619 1076–1080 (2009).
620 9. J. V Lee, A. Carrer, S. Shah, N. W. Snyder, S. Wei, S. Venneti, A. J. Worth, Z. F. Yuan, H.
621 W. Lim, S. Liu, E. Jackson, N. M. Aiello, N. B. Haas, T. R. Rebbeck, A. Judkins, K. J.
622 Won, L. A. Chodosh, B. A. Garcia, B. Z. Stanger, M. D. Feldman, I. A. Blair, K. E.
623 Wellen, Akt-dependent metabolic reprogramming regulates tumor cell Histone acetylation.
624 *Cell Metab.* **20**, 306–319 (2014).
625 10. S. Sivanand, S. Rhoades, Q. Jiang, J. V Lee, J. Benci, J. Zhang, S. Yuan, I. Viney, S. Zhao,
626 A. Carrer, M. J. Bennett, A. J. Minn, A. M. Weljie, R. A. Greenberg, K. E. Wellen,
627 Nuclear Acetyl-CoA Production by ACLY Promotes Homologous Recombination. *Mol.*
628 *Cell*. **67**, 252--265.e6 (2017).
629 11. H. F. Yancy, J. A. Mason, S. Peters, C. E. T. Iii, G. K. Littleton, M. Jett, A. A. Day,
630 Metastatic progression and gene expression between breast cancer cell lines from African
631 American and Caucasian women. *J. Carcinog.* **6** (2007), doi:10.1186/1477-3163-6-8.
632 12. E. D. Pope, E. O. Kimbrough, L. P. Vemireddy, P. K. Surapaneni, J. A. Copland, K. Mody,
633 Aberrant lipid metabolism as a therapeutic target in liver cancer. *Expert Opin. Ther.*
634 *Targets*. **23**, 473–483 (2019).
635 13. J. Turyn, B. Schlichtholz, A. Dettlaff-Pokora, M. Presler, E. Goyke, M. Matuszewski, Z.
636 Kmieć, K. Krajka, J. Swierczynski, Increased Activity of Glycerol 3-phosphate
637 Dehydrogenase and Other Lipogenic Enzymes in Human Bladder Cancer. *Horm. Metab.*
638 *Res.* **35**, 565–569 (2003).

639 14. A. Varis, M. Wolf, O. Monni, M. Vakkari, A. Kokkola, C. Moskaluk, H. Frierson, S. M.
640 Powell, S. Knuutila, A. Kallioniemi, W. El-rifai, Targets of Gene Amplification and
641 Overexpression at 17q in Gastric Cancer 1. *Cancer Res.* **62**, 2625–2629 (2002).
642 15. Y. Zhou, L. R. Bollu, F. Tozzi, X. Ye, R. Bhattacharya, G. Gao, E. Dupre, L. Xia, J. Lu, F.
643 Fan, S. Bellister, L. M. Ellis, Z. Weihua, ATP citrate lyase mediates resistance of
644 colorectal cancer cells to SN38. *Mol. Cancer Ther.* **12**, 2782–2791 (2013).
645 16. M. E. Beckner, W. Fellows-Mayle, Z. Zhang, N. R. Agostino, J. A. Kant, B. W. Day, I. F.
646 Pollack, Identification of ATP Citrate Lyase as a Positive Regulator of Glycolytic Function
647 in Glioblastomas. *Int. J. Cancer*. **126**, 2282–2295 (2011).
648 17. T. Migita, T. Narita, K. Nomura, E. Miyagi, F. Inazuka, M. Matsuura, M. Ushijima, T.
649 Mashima, H. Seimiya, Y. Satoh, S. Okumura, K. Nakagawa, Y. Ishikawa, ATP Citrate
650 Lyase : Activation and Therapeutic Implications in Non–Small Cell Lung Cancer. *Cancer*
651 *Res.* **68**, 8547–8555 (2008).
652 18. X. Qian, J. Hu, J. Zhao, H. Chen, ATP citrate lyase expression is associated with advanced
653 stage and prognosis in gastric adenocarcinoma. *Int. J. Clin. Exp. Med.* **8**, 7855–7860
654 (2015).
655 19. C. Sullivan, J. G. Hamilton, R. Wheatley, C. River, B. Laboratories, Inhibition of
656 Lipogenesis in Rat Liver by (-)Hydroxycitrate. *Arch. Biochem. Biophys.* **150**, 183–190
657 (1972).
658 20. J. M. Lowenstein, Effect of (-)Hydroxycitrate on Fatty Acid Synthesis by Rat Liver in
659 Vivo. *J. Biol. Chem.* **246**, 629–632 (1971).
660 21. S. L. Pinkosky, S. Filippov, R. A. K. Srivastava, J. C. Hanselman, C. D. Bradshaw, T. R.
661 Hurley, C. T. Cramer, M. A. Spahr, A. F. Brant, J. L. Houghton, C. Baker, M. Naples, K.
662 Adeli, R. S. Newton, AMP-activated protein kinase and ATP-citrate lyase are two distinct
663 molecular targets for ETC-1002, a novel small molecule regulator of lipid and
664 carbohydrate metabolism. *J. Lipid Res.* **54**, 134–151 (2013).
665 22. D. E. Bauer, G. Hatzivassiliou, F. Zhao, C. Andreadis, C. B. Thompson, ATP citrate lyase
666 is an important component of cell growth and transformation. *Oncogene*. **24**, 6314–6322
667 (2005).
668 23. K. S. Lucenay, I. Doostan, C. Karakas, T. Bui, Z. Ding, G. B. Mills, K. K. Hunt, K.
669 Keyomarsi, Cyclin E Associates with the Lipogenic Enzyme ATP-Citrate Lyase to Enable
670 Malignant Growth of Breast Cancer Cells. *Cancer Res.* **76**, 2406–2419 (2016).
671 24. N. Zaidi, I. Royaux, J. V Swinnen, K. Smans, ATP Citrate Lyase Knockdown Induces
672 Growth Arrest and Apoptosis through Different Cell- and Environment- Dependent
673 Mechanisms. *Mol. Cancer Ther.* **11**, 1925–1936 (2012).
674 25. G. Hatzivassiliou, F. Zhao, D. E. Bauer, C. Andreadis, A. N. Shaw, D. Dhanak, S. R.
675 Hingorani, D. A. Tuveson, C. B. Thompson, ATP citrate lyase inhibition can suppress
676 tumor cell growth. *Cancer Cell*. **8**, 311–321 (2005).
677 26. D. Wang, L. Yin, J. Wei, Z. Yang, ATP citrate lyase is increased in human breast cancer ,
678 depletion of which promotes apoptosis. *Tumor Biol.* (2017),
679 doi:10.1177/1010428317698338.
680 27. C. M. Metallo, P. A. Gameiro, E. L. Bell, K. R. Mattaini, J. Yang, K. Hiller, C. M. Jewell,
681 Z. R. Johnson, D. J. Irvine, L. Guarente, J. K. Kelleher, M. G. Vander, Reductive
682 glutamine metabolism by IDH1 mediates lipogenesis under hypoxia. *Nature*. **481**, 380–384
683 (2012).
684 28. M. G. Badur, T. Muthusamy, S. J. Parker, S. Ma, K. Mcbrayer, T. Cordes, J. H. Magana,
685 K. Guan, M. Christian, Oncogenic R132 IDH1 Mutations Limit NADPH for De Novo
686 Lipogenesis through (D)2-Hydroxyglutarate Production in Fibrosarcoma Cells. *Cell Rep.*
687 **25**, 1018–1026 (2018).
688 29. Z. T. Schug, J. Vande Voorde, E. Gottlieb, The metabolic fate of acetate in cancer. *Nat.*

689 *Publ. Gr.* **16**, 708–717 (2016).
690 30. T. Fujino, J. Kondo, M. Ishikawa, K. Morikawa, T. T. Yamamoto, Acetyl-CoA Synthetase
691 2, a Mitochondrial Matrix Enzyme Involved in the Oxidation of Acetate. *J. Biol. Chem.*
692 **276**, 11420–11426 (2001).
693 31. Z. T. Schug, B. Peck, D. T. Jones, Q. Zhang, S. Grosskurth, I. S. Alam, L. M. Goodwin, E.
694 Smethurst, S. Mason, K. Blyth, L. McGarry, D. James, E. Shanks, G. Kalna, R. E.
695 Saunders, M. Jiang, M. Howell, F. Lassailly, M. Z. Thin, B. Spencer-Dene, G. Stamp, N. J.
696 F. van den Broek, G. Mackay, V. Bulusu, J. J. Kamphorst, S. Tardito, D. Strachan, A. L.
697 Harris, E. O. Aboagye, S. E. Critchlow, M. J. O. Wakelam, A. Schulze, E. Gottlieb,
698 Acetyl-CoA synthetase 2 promotes acetate utilization and maintains cancer cell growth
699 under metabolic stress. *Cancer Cell*. **27**, 57–71 (2015).
700 32. S. A. Comerford, Z. Huang, X. Du, Y. Wang, L. Cai, A. K. Witkiewicz, H. Walters, M. N.
701 Tantawy, A. Fu, H. C. Manning, J. D. Horton, R. E. Hammer, S. L. Mcknight, B. P. Tu,
702 Acetate dependence of tumors. *Cell*. **159**, 1591–1602 (2014).
703 33. T. Mashimo, K. Pichumani, V. Vemireddy, K. J. Hatanpaa, D. K. Singh, S. Sirasanagandla,
704 S. Nannepaga, S. G. Piccirillo, Z. Kovacs, C. Foong, Z. Huang, S. Barnett, B. E. Mickey,
705 R. J. Deberardinis, B. P. Tu, E. A. Maher, R. M. Bachoo, Acetate is a bioenergetic
706 substrate for human glioblastoma and brain metastases. *Cell*. **159**, 1603–1614 (2014).
707 34. J. J. Kamphorst, M. K. Chung, J. Fan, J. D. Rabinowitz, Quantitative analysis of acetyl-
708 CoA production in hypoxic cancer cells reveals substantial contribution from acetate.
709 *Cancer Metab.* **2**, 23 (2014).
710 35. B. Yenilmez, M. Kelly, G. Zhang, N. Wetoska, O. R. Ilkayeva, K. Min, L. Rowland, C.
711 DiMarzio, W. He, N. Raymond, L. Lifshitz, M. Pan, X. Han, J. Xie, R. H. Friedline, J. K.
712 Kim, G. Gao, M. A. Herman, C. B. Newgard, M. P. Czech, Paradoxical activation of
713 transcription factor SREBP1c and de novo lipogenesis by hepatocyte-selective ATP-citrate
714 lyase depletion in obese mice. *J. Biol. Chem.*, 102401 (2022).
715 36. S. Zhao, A. M. Torres, R. A. Henry, S. Trefely, M. Wallace, J. V Lee, A. Carrer, A.
716 Sengupta, S. L. Campbell, Y. M. Kuo, A. J. Frey, N. Meurs, J. M. Viola, I. A. Blair, A. M.
717 Weljie, C. M. Metallo, N. W. Snyder, A. J. Andrews, K. E. Wellen, ATP-Citrate Lyase
718 Controls a Glucose-to-Acetate Metabolic Switch. *Cell Rep.* **17**, 1037–1052 (2016).
719 37. F. Bian, T. Kasumov, K. K. Thomas, K. A. Jobbins, F. David, P. E. Minkler, C. L. Hoppel,
720 H. Brunengraber, Peroxisomal and mitochondrial oxidation of fatty acids in the heart,
721 assessed from the 13C labeling of malonyl-CoA and the acetyl moiety of citrate. *J. Biol.*
722 *Chem.* **280**, 9265–9271 (2005).
723 38. A. E. Reszko, T. Kasumov, F. David, K. A. Jobbins, K. R. Thomas, C. L. Hoppel, H.
724 Brunengraber, C. Des Rosiers, Peroxisomal Fatty Acid Oxidation Is a Substantial Source of
725 the Acetyl Moiety of Malonyl-CoA in Rat Heart. *J. Biol. Chem.* **279**, 19574–19579 (2004).
726 39. T. Kasumov, J. E. Adams, F. Bian, F. David, K. R. Thomas, K. A. Jobbins, P. E. Minkler,
727 C. L. Hoppel, H. Brunengraber, Probing peroxisomal β-oxidation and the labelling of
728 acetyl-CoA proxies with [1-13C]octanoate and [3-13C]octanoate in the perfused rat liver.
729 *Biochem. J.* **389**, 397–401 (2005).
730 40. A. He, X. Chen, M. Tan, Y. Chen, D. Lu, X. Zhang, J. M. Dean, B. Razani, I. J. Lodhi,
731 Acetyl-CoA Derived from Hepatic Peroxisomal $β$-Oxidation Inhibits Autophagy and
732 Promotes Steatosis via mTORC1 Activation. *Mol. Cell*. **79**, 30–42 (2020).
733 41. S. Zha, S. Ferdinandusse, J. L. Hicks, S. Denis, T. A. Dunn, R. J. Wanders, J. Luo, A. M.
734 De Marzo, W. B. Isaacs, Peroxisomal branched chain fatty acid β-oxidation pathway is
735 upregulated in prostate cancer. *Prostate*. **63** (2005), pp. 316–323.
736 42. L. Jiang, A. A. Shestov, P. Swain, C. Yang, S. J. Parker, Q. A. Wang, L. S. Terada, N. D.
737 Adams, M. T. Mccabe, B. Pietrak, S. Schmidt, C. M. Metallo, B. P. Dranka, B. Schwartz,
738 R. J. Deberardinis, Reductive carboxylation supports redox homeostasis during anchorage-

739 independent growth. *Nature*. **532**, 255–258 (2016).
740 43. J. Son, C. A. Lyssiotis, H. Ying, X. Wang, S. Hua, M. Ligorio, R. M. Perera, C. R. Ferrone,
741 E. Mullarky, N. Shyh-Chang, Y. Kang, J. B. Fleming, N. Bardeesy, J. M. Asara, M. C.
742 Haigis, R. A. Depinho, L. C. Cantley, A. C. Kimmelman, Glutamine supports pancreatic
743 cancer growth through a KRAS-regulated metabolic pathway. *Nature*. **496**, 101–105
744 (2013).
745 44. A. Kumar, T. Cordes, A. E. Thalacker-Mercer, A. M. Pajor, A. N. Murphy, C. M. Metallo,
746 NaCT/SLC13A5 facilitates citrate import and metabolism under nutrient-limited
747 conditions. *Cell Rep.* **36**, 109701 (2021).
748 45. X. Gao, S. Lin, F. Ren, J. Li, J. Chen, C. Yao, H. Yang, S. Jiang, G. Yan, D. Wang, Y.
749 Wang, Y. Liu, Z. Cai, Y. Xu, J. Chen, W. Yu, P. Yang, Q. Lei, Acetate functions as an
750 epigenetic metabolite to promote lipid synthesis under hypoxia. *Nat. Commun.* **7**, 1–14
751 (2016).
752 46. W. S. Yang, K. J. Kim, M. M. Gaschler, M. Patel, M. S. Shchepinov, B. R. Stockwell,
753 Peroxidation of polyunsaturated fatty acids by lipoxygenases drives ferroptosis. *Proc. Natl.*
754 *Acad. Sci. U. S. A.* **113**, E4966--E4975 (2016).
755 47. O. Feron, The many metabolic sources of acetyl-CoA to support histone acetylation and
756 influence cancer progression. *Ann. Transl. Med.* **7**, S277--S277 (2019).
757 48. M. Wallace, C. R. Green, L. S. Roberts, Y. M. Lee, J. L. McCarville, J. Sanchez-
758 Gurmaches, N. Meurs, J. M. Gengatharan, J. D. Hover, S. A. Phillips, T. P. Ciaraldi, D. A.
759 Guertin, P. Cabrales, J. S. Ayres, D. K. Nomura, R. Loomba, C. M. Metallo, Enzyme
760 promiscuity drives branched-chain fatty acid synthesis in adipose tissues. *Nat. Chem. Biol.*
761 **14**, 1021–1031 (2018).
762 49. L. Izzo1, The carnitine shuttle links mitochondrial metabolism to histone acetylation and
763 lipogenesis. *Co-submitted* (2022).
764 50. X. Liu, D. E. Cooper, A. A. Cluntun, M. O. Warmoes, S. Zhao, M. A. Reid, J. Liu, P. J.
765 Lund, M. Lopes, B. A. Garcia, K. E. Wellen, D. G. Kirsch, J. W. Locasale, Acetate
766 Production from Glucose and Coupling to Mitochondrial Metabolism in Mammals. *Cell*.
767 **175**, 502--513.e13 (2018).
768 51. I. J. Lodhi, C. F. Semenkovich, Peroxisomes: A nexus for lipid metabolism and cellular
769 signaling. *Cell Metab.* **19**, 380–392 (2014).
770 52. O. Apanasets, C. P. Grou, P. P. Van Veldhoven, C. Brees, B. Wang, M. Nordgren, G.
771 Dodt, J. E. Azevedo, M. Fransen, PEX5, the Shuttling Import Receptor for Peroxisomal
772 Matrix Proteins, Is a Redox-Sensitive Protein. *Traffic*. **15**, 94–103 (2014).
773 53. C. Van den Branden, F. Roels, Thioridazine: a selective inhibitor of peroxisomal β-
774 oxidation in vivo. *FEBS Lett.* **187**, 331–333 (1985).
775 54. R. Shi, Y. Zhang, Y. Shi, S. Shi, L. Jiang, Inhibition of peroxisomal β-oxidation by
776 thioridazine increases the amount of VLCFAs and Aβ generation in the rat brain. *Neurosci.*
777 *Lett.* **528**, 6–10 (2012).
778 55. R. J. A. Wanders, H. R. Waterham, S. Ferdinandusse, Metabolic interplay between
779 peroxisomes and other subcellular organelles including mitochondria and the endoplasmic
780 reticulum. *Front. Cell Dev. Biol.* **3**, 1–15 (2016).
781 56. B. S. Jakobs, R. J. A. Wanders, Fatty acid $β$-oxidation in peroxisomes and mitochondria:
782 The first, unequivocal evidence for the involvement of carnitine in shuttling propionyl-
783 CoA from peroxisomes to mitochondria. *Biochem. Biophys. Res. Commun.* **213** (1995), pp.
784 1035–1041.
785 57. F. Leighton, S. Bergseth, T. Rortveit, E. N. Christiansen, J. Bremer, Free acetate
786 production by rat hepatocytes during peroxisomal fatty acid and dicarboxylic acid
787 oxidation. *J. Biol. Chem.* **264**, 10347–10350 (1989).
788 58. J. Hsu, N. Fatuzzo, N. Weng, W. Michno, W. Dong, M. Kienle, Y. Dai, A. Pasca, M. Abu-

789 Remaileh, N. Rasgon, B. Bigio, C. Nasca, C. Khosla, Carnitine octanoyltransferase is
790 important for the assimilation of exogenous acetyl-L-carnitine into acetyl-CoA in
791 mammalian cells. *J. Biol. Chem.*, 102848 (2022).
792 59. Y. Il Kim, I. K. Nam, D. K. Lee, S. Bhandari, L. Charton, S. A. Kwak, J. Y. Lim, K. H.
793 Hong, S. J. Kim, J. N. Lee, S. W. Kwon, H. S. So, N. Linka, R. Park, S. K. Choe, Slc25a17
794 acts as a peroxisomal coenzyme A transporter and regulates multiorgan development in
795 zebrafish. *J. Cell. Physiol.* **235**, 151–165 (2020).
796 60. A. Baker, D. J. Carrier, T. Schaedler, H. R. Waterham, C. W. Van Roermund, F. L.
797 Theodoulou, Peroxisomal ABC transporters: Functions and mechanism. *Biochem. Soc.*
798 *Trans.* **43**, 959–965 (2015).
799 61. A. Carrer, S. Trefely, S. Zhao, S. L. Campbell, R. J. Norgard, K. C. Schultz, S. Sidoli, J. L.
800 D. Parris, H. C. Affronti, S. Sivanand, S. Egolf, Y. Sela, M. Trizzino, A. Gardini, B. A.
801 Garcia, N. W. Snyder, B. Z. Stanger, K. E. Wellen, Acetyl-CoA metabolism supports
802 multistep pancreatic tumorigenesis. *Cancer Discov.* **9**, 416–435 (2019).
803 62. J. M. Bae, J. H. Kim, H. J. Oh, H. E. Park, T. H. Lee, N. Cho, G. H. Kang, Downregulation
804 of acetyl-CoA synthetase 2 is a metabolic hallmark of tumor progression and
805 aggressiveness in colorectal carcinoma. **30**, 267–277 (2016).
806 63. V. Bulusu, S. Tumanov, E. Michalopoulou, N. J. Van Den Broek, G. Mackay, C. Nixon, S.
807 Dhayade, Z. T. Schug, J. Vande Voorde, K. Blyth, E. Gottlieb, A. Vazquez, J. J.
808 Kamphorst, Acetate Recapturing by Nuclear Acetyl-CoA Synthetase 2 Prevents Loss of
809 Histone Acetylation during Oxygen and Serum Limitation Article Acetate Recapturing by
810 Nuclear Acetyl-CoA Synthetase 2 Prevents Loss of Histone Acetylation during Oxygen
811 and Serum Limi. *Cell Rep.* **18**, 647–658 (2017).
812 64. L. Yao, L. Jiang, F. Zhang, M. Li, B. Yang, F. Zhang, X. Guo, Acetate promotes SNAI1
813 expression by ACSS2-mediated histone acetylation under glucose limitation in renal cell
814 carcinoma cell. *Biosci. Rep.* **40**, 1–10 (2020).
815 65. S. Trefely, C. D. Lovell, N. W. Snyder, K. E. Wellen, Compartmentalised acyl-CoA
816 metabolism and roles in chromatin regulation. *Mol. Metab.* **38**, 100941 (2020).
817 66. A. Luengo, D. Y. Gui, M. G. Vander Heiden, Targeting Metabolism for Cancer Therapy.
818 *Cell Chem. Biol.* **24**, 1161–1180 (2017).
819 67. C. W. T. Van Roermund, E. H. Hettema, M. Van Den Berg, H. F. Tabak, R. J. A. Wanders,
820 Molecular characterization of carnitine-dependent transport of acetyl-CoA from
821 peroxisomes to mitochondria in Saccharomyces cerevisiae and identification of a plasma
822 membrane carnitine transporter, Agp2p. *EMBO J.* **18**, 5843–5852 (1999).
823 68. S. M. Houten, R. J. A. Wanders, P. Ranea-Robles, Metabolic interactions between
824 peroxisomes and mitochondria with a special focus on acylcarnitine metabolism. *Biochim.*
825 *Biophys. Acta - Mol. Basis Dis.* **1866**, 165720 (2020).
826 69. J. D. Young, INCA: A computational platform for isotopically non-stationary metabolic
827 flux analysis. *Bioinformatics*. **30**, 1333–1335 (2014).
828 70. T. Cordes, C. M. Metallo, "Quantifying Intermediary Metabolism and Lipogenesis in
829 Cultured Mammalian Cells Using Stable Isotope Tracing and Mass Spectrometry" in *High-*
830 *Throughput Metabolomics: Methods and Protocols*, A. D'Alessandro, Ed. (Springer New
831 York, New York, NY, 2019; https://doi.org/10.1007/978-1-4939-9236-2_14), pp. 219–241.
832 71. F. A. Ran, P. D. Hsu, J. Wright, V. Agarwala, D. A. Scott, F. Zhang, Genome engineering
833 using the CRISPR-Cas9 system. *Nat. Protoc.* **8**, 2281–2308 (2013).
834 72. N. E. Sanjana, O. Shalem, F. Zhang, Improved vectors and genome-wide libraries for
835 CRISPR screening. *Nat. Methods*. **11**, 783–784 (2014).
836 73. S. Kim, D. Kim, S. W. Cho, J. Kim, J. S. Kim, Highly efficient RNA-guided genome
837 editing in human cells via delivery of purified Cas9 ribonucleoproteins. *Genome Res.* **24**,
838 1012–1019 (2014).

74. A. Kumar, J. Mitchener, Z. A. King, C. M. Metallo, Escher-Trace: A web application for pathway-based visualization of stable isotope tracing data. *BMC Bioinformatics*. **21**, 1–10 (2020).

Acknowledgments

We thank all members of the Metallo laboratory for support and helpful discussions. We thank Dr. Steven Zhao for helping with generating PEX5KO cell lines. ACLY and ACSS2 cellular reagents were provided by Nimbus Therapeutics. Figure panels were made with Biorender. **Funding:** This work was supported by US National Institutes of Health (NIH) grants R35CA220538 and P01CA120964 (to R.J.S.) and R01CA234245 (to C.M.M.). A.K. was supported in part by U54CA132379, and H.G. was supported in part by T32DK007541. **Author contributions:** R.K., A.K., R.U.S. and C.M.M. conceived and designed the study. R.K. and A.K. performed experiments. R.K. generated the *PEX5*-KO cell lines. H.G. and R.J.S. provided 643T cell lines and advised on studies. R.K., G.H.M., and C.R.G. performed LC-MS/MS lipidomic analytics. T.C. performed the ferroptosis assay. R.K., A.K., and C.M.M wrote the paper with input from all authors. **Competing interests:** The authors declare no competing interests. **Data and materials availability:** All data needed to evaluate the conclusions in the paper are present in the paper and/or the Supplementary Materials.

Figures:

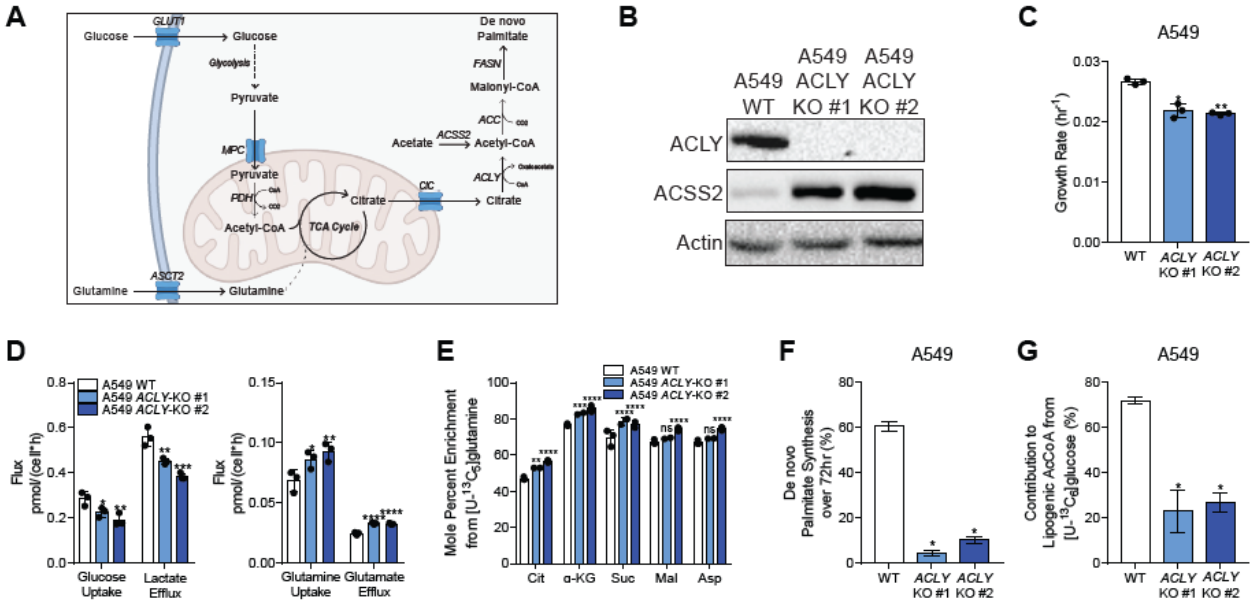

Figure 1. ACLY-KO rewires central carbon metabolism and leads to a reduction of palmitate synthesis in cancer cells

(A) Canonical de novo lipogenesis pathway

(B) Western Blots of ACLY, ACSS2, and actin in A549 WT and ACLY-KO cells.

(C) Growth rates of A549 WT and ACLY-KO cells grown in high glucose DMEM +10% FBS for 4 days.

(D) Glucose uptake, lactate efflux (left) and glutamine uptake, glutamate efflux (right) in A549 WT and ACLY-KO cells cultured in high glucose DMEM +10% dFBS for 72 hours (n=3).

(E) Mole percent enrichment of TCA intermediates from [U-13C5]glutamine in A549 ACLY-KO clones cultured in high glucose DMEM +10% dFBS for 72 hours (n=3).

(F) De novo synthesis of palmitate in A549 ACLY-KO cells cultured in high glucose DMEM +10% dFBS for 72 hours (n=3).

(G) Percent of lipogenic acetyl-CoA contributed by [U-13C6]glucose based on ISA modeling in A549 ACLY-KO cells cultured in high glucose DMEM +10% dFBS 72 hours (n=3).

In (C-G) data are plotted as mean ± SD. Statistical significance is relative to WT as determined by One-way ANOVA w/ Dunnet's method for multiple comparisons (C-E) with *, P value < 0.05; **, P value < 0.01; ***, P value < 0.001, ****, P value < 0.0001. In (F,G) *data are plotted as mean estimated flux +/- 95% confidence intervals generated via parameter continuation in INCA. Unless indicated, all data represent biological triplicates. Data shown are from one of at least two separate experiments. See also Figure S1.

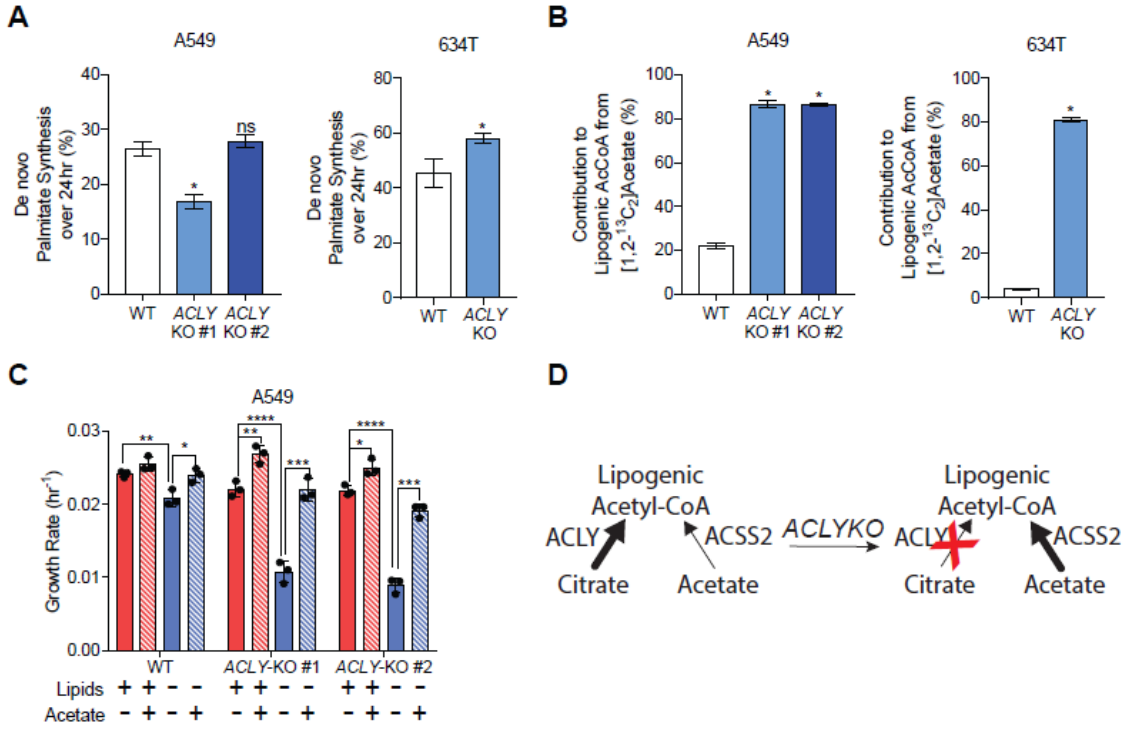

Figure 2. ACLY-KO growth and fatty acid synthesis is rescued with addition of extracellular acetate

(A) De novo synthesis of palmitate in A549 (left) and 634T (right) WT and ACLY-KO cells cultured in high glucose DMEM +10% Dfbs + 1 mM acetate for 24 hours (n=3).

(B) Percent of lipogenic acetyl-CoA contributed by [1,2-13C2]acetate in A549 (left) and 634T (right) and ACLY-KO cells cultured in high glucose DMEM +10% dFBS + 1 mM acetate for 24 hours (n=3).

(C) Growth rates of A549 WT and ACLY-KO cells grown in high glucose DMEM +10% dFBS or delipidated dFBS +/- 1 mM acetate for 4 days (n=3).

(D) Schematic of lipogenic acetyl-CoA synthesis in ACLY-KO cells.

In (A,B) *data are plotted as mean estimated flux +/- 95% confidence intervals generated via parameter continuation in INCA. In (C) data are plotted as mean ± SD. Statistical significance is determined by Two-way ANOVA w/ Tukey's method for multiple comparisons with *, P value < 0.05; **, P value < 0.01; ***, P value < 0.001, ****, P value < 0.0001. Unless indicated, all data represent biological triplicates. Data shown are from one of at least two separate experiments. See also Figure S2.

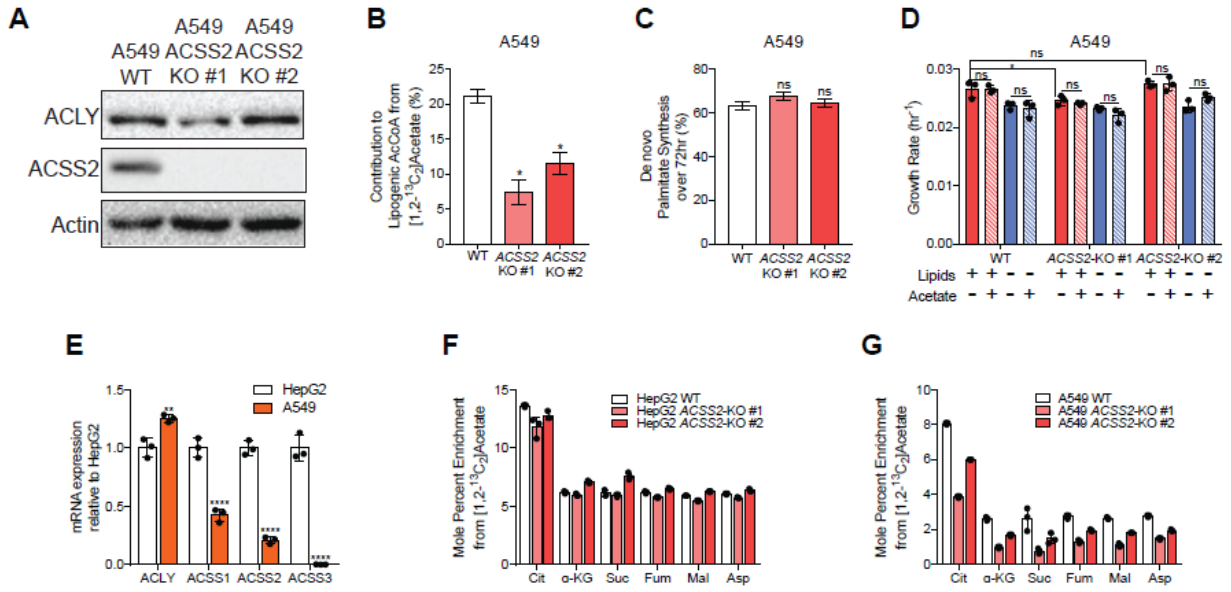

Figure 3. ACSS2-KO attenuates catabolism of exogenous acetate with minimal effect on glucose catabolism

(A) Western Blots of ACLY, ACSS2, and actin in A549 WT and ACSS2-KO cells.
(B) Percent of lipogenic acetyl-CoA contributed by [1,2-13C2] acetate based on ISA modeling in A549 ACSS2-KO cells cultured in high glucose DMEM +10% dFBS + 1 mM acetate for 24 hours (n=3).
(C) De novo synthesis of palmitate in A549 ACSS2-KO cells cultured in high glucose DMEM +10% dFBS for 72 hours (n=3).
(D) Growth rates of A549 WT and ACSS2-KO cells grown in high glucose DMEM +10% dFBS or delipidated dFBS +/- 1 mM acetate for 4 days (n=3).
(E) mRNA expression of acetyl-CoA generating enzymes in HepG2 and A549 cells (n=3).
(F) Mole percent enrichment of TCA intermediates from [1,2-13C2] acetate in HepG2 ACSS2-KO cells cultured in high glucose DMEM +10% dFBS + 1 mM acetate for 24 hours (n=3).
(G) Mole percent enrichment of TCA intermediates from [1,2-13C2] acetate in A549 ACSS2-KO cells cultured in high glucose DMEM +10% dFBS + 1 mM acetate for 24 hours (n=3).
In (B, C) *data are plotted as mean estimated flux +/- 95% confidence intervals generated via parameter continuation in INCA. In (D-G) data are plotted as mean ± SD. Statistical significance is determined by Two-way ANOVA w/ Tukey's method for multiple comparisons (D); or relative to HepG2 as determined by two-sided Student's t-test (G) with *, P value < 0.05; **, P value < 0.01; ***, P value < 0.001, ****, P value < 0.0001. Unless indicated, all data represent biological triplicates. Data shown are from one of at least two separate experiments. See also Figure S3.

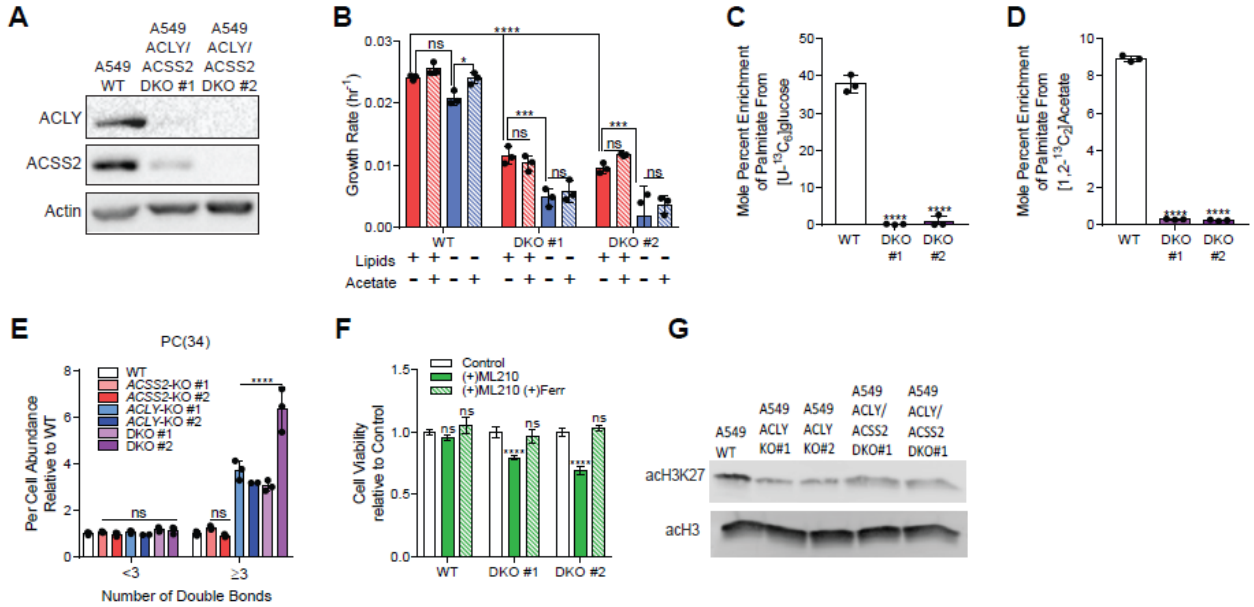

Figure 4. ACLY/ACSS2-DKO cells are reliant on extracellular lipids, with minimal change in protein acetylation.

(A) Western Blots of ACLY, ACSS2, and actin in A549 WT and ACLY/ACSS2-DKO cells.
(B) Growth rates of A549 WT and ACLY/ACSS2-DKO cells grown in high glucose DMEM +10% dFBS or delipidated dFBS +/- 1 mM acetate for 4 days (n=3).
(C) Mole percent enrichment of palmitate from [U-13C6] glucose in A549 ACLY/ACSS2-DKO cells cultured in high glucose DMEM +10% dFBS for 72 hours (n=3).
(D) Mole percent enrichment of palmitate from [1,2-13C2] acetate in A549 ACLY/ACSS2-DKO cells cultured in high glucose DMEM +10% dFBS + 1 mM acetate for 24 hours (n=3).
(E) PC(34) abundance of A549 WT, ACSS2-KO, ACLY-KO, ACLY/ACSS2-DKO cells cultured in high glucose DMEM +10% FBS for 2 days (n=3).
(F) Cell viability of A549 WT and ACLY/ACSS2-DKO cells cultured in DMEM+10% dFBS +/- 2 μM ML210 and/or 2 μM Ferrostatin for 48 hours (n=4).
(G) Acid extracted histone western blot from A549 WT, ACLY-KO, ACLY/ACSS2 DKO cells cultured in DMEM + 10% FBS 24 hours (n=3).
In (B-F) data are plotted as mean ± SD. Statistical significance is determined by Two-way ANOVA w/ Tukey's method for multiple comparisons (B); or relative to WT as determined by One-way ANOVA w/ Dunnet's method for multiple comparisons (C-F) with *, P value < 0.05; **, P value < 0.01; ***, P value < 0.001, ****, P value < 0.0001. Unless indicated, all data represent biological triplicates. Data shown are from one of at least two separate experiments. See also Figure S4.

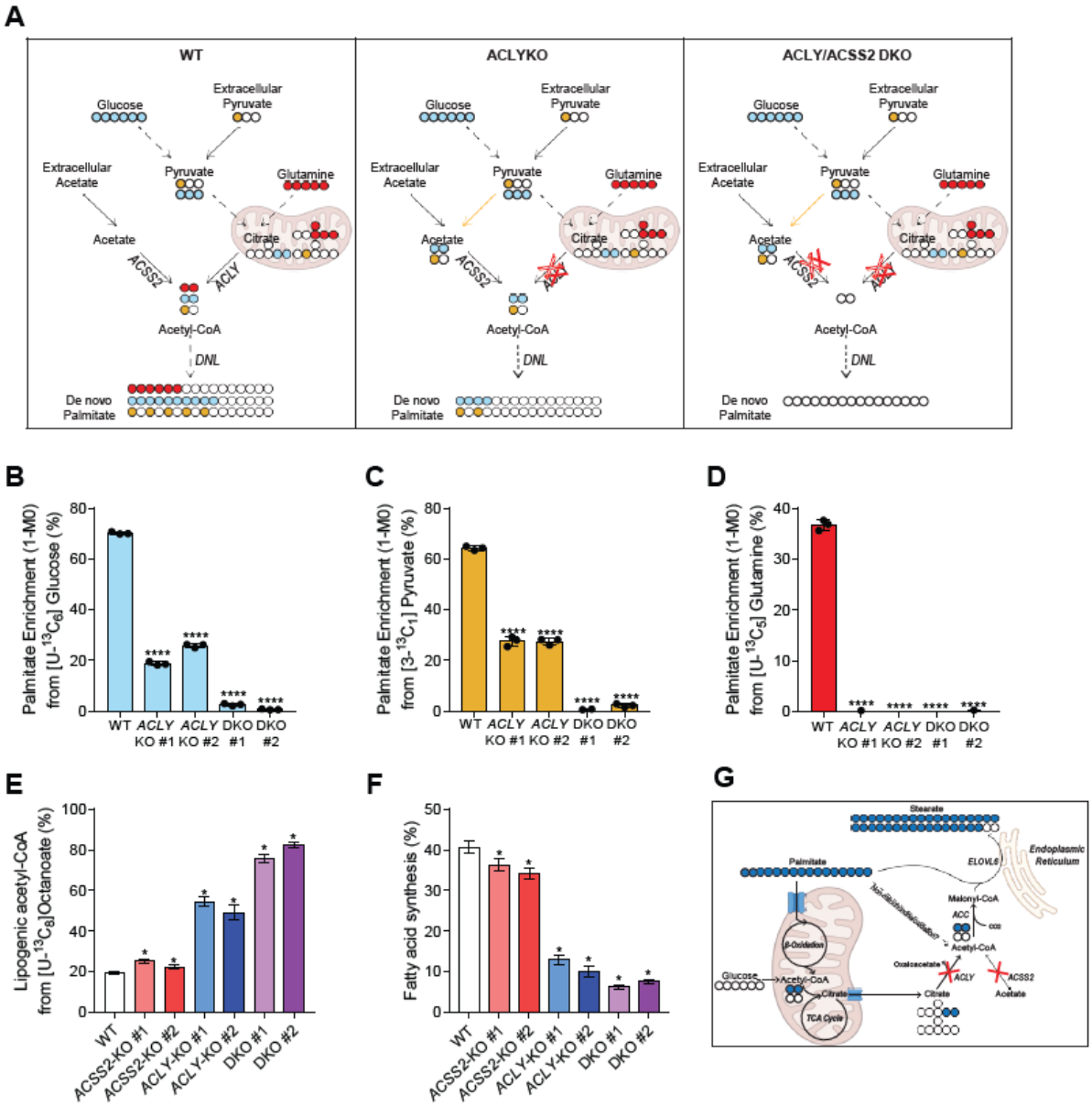

Figure 5. Disruption of canonical acetyl-CoA synthesis induces alternative synthesis pathways

(A) Schematic showing de novo acetate synthesis in ACLY-KO cells. Dashed lines represent multiple reactions.

(B) Enrichment (1-M0) of palmitate from [U-13C6] glucose in A549 WT, ACLY-KO, ACLY/ACSS2-DKO cells cultured in high glucose DMEM +10% dFBS for 72 hours (n=3).

(C) Enrichment (1-M0) of palmitate from [3-13C1] pyruvate in A549 WT, ACLY-KO, ACLY/ACSS2-DKO cells cultured in high glucose DMEM +10% dFBS + 5mM pyruvate for 72 hours (n=3).

(D) Enrichment (1-M0) of palmitate from [U-13C5] glutamine in A549 WT, ACLY-KO, ACLY/ACSS2-DKO cells cultured in high glucose DMEM +10% dFBS for 72 hours (n=3).

(E) Percent of lipogenic acetyl-CoA contributed by [U-13C8] octanoate based on ISA modeling in A549 WT, ACSS2-KO, ACLY-KO, ACLY/ACSS2-DKO cells cultured in high glucose DMEM +10% dFBS + 500 µM octanoate for 24 hours (n=3).

1008 (F) De novo synthesis of palmitate in A549 WT, ACSS2-KO, ACLY-KO, ACLY/ACSS2-DKO
1009 cells cultured in high glucose DMEM +10% dFBS + 500 μM octanoate for 24 hours (n=3).
1010 (G) Schematic of Nnon-mitochondrial acetyl-CoA synthesis from [U-13C8]octanoate in
1011 ACLY/ACSS2-DKO cells. Filled circles are 13C, empty circles are 12C.
1012 In (B-F) data are plotted as mean ± SD. Statistical significance relative to WT as determined by
1013 One-way ANOVA w/ Dunnet's method for multiple comparisons (B-D) with *, P value < 0.05;
1014 **, P value < 0.01; ***, P value < 0.001, ****, P value < 0.0001. In (E-F) *data are
1015 plotted as mean estimated flux +/- 95% confidence intervals generated via parameter continuation
1016 in INCA. Unless indicated, all data represent biological triplicates. Data shown are from one of at
1017 least two separate experiments. See also Figure S5.
1018

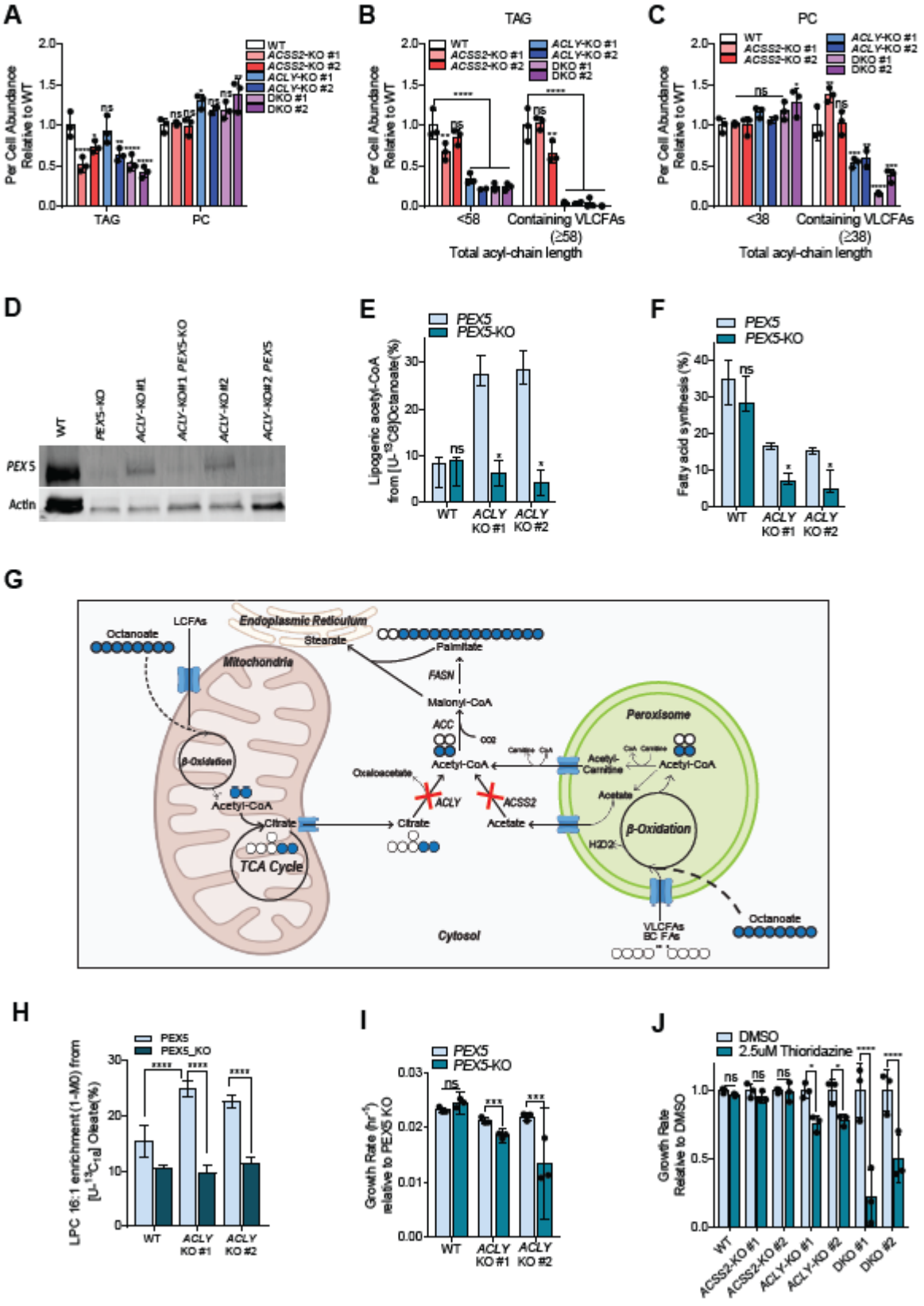
A
Per Cell Abundance Relative to WT
WT
ACSS2-KO #1
ACSS2-KO #2
ACLY-KO #1
ACLY-KO #2
DKO #1
DKO #2
TAG
PC
B
TAG
<58
Containing VLCFAs (≥58)
Total acyl-chain length
C
PC
<38
Containing VLCFAs (≥38)
Total acyl-chain length
D
WT
PEX5-KO
ACLY-KO#1
ACLY-KO#1 PEX5-KO
ACLY-KO#2
ACLY-KO#2 PEX5
PEX5
Actin
E
PEX5
PEX5-KO
Lipogenic acetyl-CoA from [U-13C8]Octanoate(%)
WT
ACLY KO #1
ACLY KO #2
F
PEX5
PEX5-KO
Fatty acid synthesis (%)
WT
ACLY KO #1
ACLY KO #2
G
Octanoate
LCFAs
Endoplasmic Reticulum
Stearate
Palmitate
Mitochondria
FASN
Malonyl-CoA
ACC
CO2
Peroxisome
β-Oxidation
Acetyl-CoA
Oxaloacetate
Acetyl-Carnitine
Acetyl-CoA
Acetate
ACLY
ACSS2
Citrate
Citrate
Acetate
β-Oxidation
H2O2
TCA Cycle
Cytosol
VLCFAs BC FAs
Octanoate
H
PEX5
PEX5_KO
LPC 16:1 enrichment (1-M0) from [U-13C16] Oleate(%)
WT
ACLY KO #1
ACLY KO #2
I
PEX5
PEX5-KO
Growth Rate (hr-1) relative to PEX5 KO
WT
ACLY KO #1
ACLY KO #2
J
DMSO
2.5uM Thioridazine
Growth Rate Relative to DMSO
WT
ACSS2-KO #1
ACSS2-KO #2
ACLY-KO #1
ACLY-KO #2
DKO #1
DKO #2

Figure 6. Peroxisomal β-oxidation becomes a major source of lipogenic acetyl-CoA with ACLYKO and ACLY/ACSS2 DKO

(A-C) Total abundance of TAGs and PCs (A), total abundance of saturated, mono- and di-unsaturated TAGs per cell (B), total abundance of saturated and monounsaturated PCs per cell (C) in A549 WT, ACSS2-KO, ACLY-KO, ACLY/ACSS2-DKO cells cultured in high glucose DMEM +10% FBS for 2 days (n=3).

(D) Western blots of PEX5 and actin in A549 WT, PEX5 KO, ACLY KO and ACLY-PEX5-KO cells.

(E-F) Percent of lipogenic acetyl-CoA contributed by [U-13C8] octanoate based on ISA modeling (E), De novo synthesis of palmitate (F) in A549 WT, PEX5-KO, ACLY-KO and ACLY/PEX-5 KO cells cultured in high glucose DMEM +10% dFBS for 48 hours (n=3).

(G) Schematic of peroxisomal acetyl-CoA synthesis from [U-13C8] octanoate in ACLY/ACSS2-DKO cells. Filled circles are 13C, empty circles are 12C.

(H) Enrichment (1-M0) of LPC from 100 μM [U-13C18] oleate in A549 WT, ACLY-KO, ACLY/PEX5-DKO cells cultured in high glucose DMEM +10% dFBS for 48 hours (n=3).

(I) Growth rates of A549 WT and ACLY-KO relative to PEX5 KO cells grown in high glucose DMEM +10% FBS for 4 days.

(J) Growth rates of A549 WT and ACLY/ACSS2-DKO cells grown in high glucose DMEM +10% dFBS +/- 2.5 μM thioridazine relative to DMSO for 4 days (n=3)

In (A-C, H-J) data are plotted as mean ± SD. Statistical significance as determined by One-way ANOVA w/ Dunnet's method for multiple comparisons relative to WT (A-C) or DMSO (J) with *, P value < 0.05; **, P value < 0.01; ***, P value < 0.001, ****, P value < 0.0001. In (E,F) data are plotted as mean ± 95% confidence interval (CI). Statistical significance by non-overlapping confidence intervals, *. Unless indicated, all data represent biological triplicates. Data shown are from one of at least two separate experiments. See also Figure S6.